FSRCC two-valence calculations of clock transition properties, dipole polarizability and isotope shifts in Fermionic and Bosonic Sr

Palki Gakkhar,[1] D. Angom,[2] and B. K. Mani[1,*]

[1]*Department of Physics, Indian Institute of Technology, Hauz Khas, New Delhi 110016, India*
[2]*Department of Physics, Manipur University, Canchipur 795003, Manipur, India*

We employ an all-particle multireference Fock-space relativistic coupled-cluster (FSRCC) theory to study the $5s^2\ ^1S_0 - 5s5p\ ^3P_0^o$ clock transition in both Fermionic and Bosonic isotopes of Sr. We compute the excitation energies for several low-lying states, E1 and M1 transition amplitudes, hyperfine reduced matrix elements, and isotope shifts using FSRCC theory. Further, using our results on E1, M1 and HFS reduced matrix elements, we calculate the lifetime of the metastable clock states for ^{87}Sr and ^{88}Sr. Furthermore, we employ perturbed relativistic coupled-cluster (PRCC) theory to compute the ground state electric dipole polarizability of Sr. To improve the accuracy of our results, we incorporate the corrections from the relativistic and quantum electrodynamical (QED) effects, and perturbative triples to all our calculations. Moreover, we employ large bases to ensure the convergence of the computed properties. Our computed excitation energies are in good agreement with the experimental data for low-lying excited states. Our results for E1, M1 and HFS reduced matrix elements are within the experimental error bars, however, with slight difference from the previous calculations due to more accurate treatment of electron correlations in our calculation. Our computed lifetime of the clock state for ^{87}Sr is within the error bars of the available experimental results, whereas for ^{88}Sr it is an order of magnitude smaller than the only available calculation [R. Santra *et al.,* Phys. Rev. A **69**, 042510 (2004)] using model potential. Our PRCC result for the ground state polarizability is in good agreement with the experiment, and smaller than previous calculations. As can be expected, our FSRCC results on isotope shift parameters show differences from the MCDF calculations. From the detailed analysis of the results, we find that the corrections from the Breit interaction, QED effects, and perturbative triples are crucial to get accurate clock transition properties in Sr. Moreover, *valence-valence* electron correlation is important to get accurate energies and properties of Sr.

I. INTRODUCTION

The unprecedented accuracy of optical atomic clocks has revolutionized the precision timekeeping which has led to several fundamental as well as technological implications across different fields [1, 2]. By using ultra-narrow optical transitions in atoms or ions, these clocks achieve high accuracy and stability, surpassing the traditional microwave frequency based clocks. This high level of precision enables new possibilities for testing the fundamental physics beyond the standard model (BSM) [3, 4], including the variation in the fundamental constants [5–7] and the tests of general relativity [8, 9]. Beyond fundamental physics, optical atomic clocks are also useful in practical applications such as geodesy [10], quantum computers [11, 12], redefining the SI unit of second [13] and navigation systems [14, 15]. Their role in advancing technologies for radar, radio astronomy, and telecommunications [14] further underscores their importance in technological applications.

Among the leading candidates for optical atomic clocks, neutral atoms and singly charged ions based clocks are at the forefront of precision timekeeping. The ion-based clocks such as ^{27}Al$^+$ [16], ^{40}Ca$^+$ [17], ^{88}Sr$^+$ [18], ^{115}In$^+$ [19], ^{171}Yb$^+$ [20], and ^{199}Hg$^+$ [21] are widely studied due to their high precision [2]. Among these, ^{27}Al$^+$ quantum logic clock currently holds the record for the highest accuracy, with a fractional frequency uncertainty of 5.5×10^{-19} [16]. Its hyperfine induced $3s^2\ ^1S_0(F = 5/2) \rightarrow 3s3p\ ^3P_0(F = 5/2)$ clock transition is reported to demonstrate a significant advancement in precision timekeeping. Among the neutral atoms clocks, lattice clocks based on ^{87,88}Sr [22, 23], ^{171}Yb [24] and ^{199}Hg [25] have gained prominence in recent years [2]. These clocks have demonstrated a remarkable accuracy and stability, pushing the boundaries of precision timekeeping. For instance, the hyperfine induced $5s^2\ ^1S_0(F = 9/2) \rightarrow 5s5p\ ^3P_0(F = 9/2)$ transition in Fermionic Sr (^{87}Sr) is reported to show an excellent balance between accuracy and practicality with a fractional frequency shift of 8.1×10^{-19} [22]. It is, perhaps, the most accurate lattice clock in existence today. It leverages thousands of neutral atoms trapped in an optical lattice, providing a superior short-term stability and low fractional frequency shifts due to environmental perturbations. Moreover, compared to Al$^+$ clocks, which face practical challenges due to complex experimental setups and limited short-term stability[26, 27], ^{87}Sr clocks require relatively simpler experimental setups [28]. In addition, the availability of series of stable isotopes allows to probe the nuclear properties and the search for the new physics beyond the standard model [29]. While studying isotope shifts between a Fermionic and Bosonic isotopes offers a unique insights into nuclear properties, examining isotope shifts among Bosonic isotopes (^{84}Sr, ^{86}Sr, ^{88}Sr) could provide important insights into the BSM physics [29]. The *two* photon E1+M1 allowed $5s^2\ ^1S_0 \rightarrow 5s5p\ ^3P_0$ clock transition in Bosonic Sr (^{88}Sr) is demonstrated to be an excellent candidate for optical clock, particularly for space-based applications [30]. The advantages with ^{88}Sr over ^{87}Sr are, a higher natural abundance (83%, as compared to only 7% for ^{87}Sr) and the absence of hyperfine splitting, which simplifies the cooling and spectroscopic processes [30]. These make ^{88}Sr a

* bkmani@physics.iitd.ac.in

suitable candidate for a robust and transportable optical lattice clock. Notably, experiments conducted with ^{88}Sr have shown remarkable performance, achieving an instability of 3×10^{-18} and a fractional frequency shift of 2×10^{-17} [30].

Despite this important prospect with Sr as an optical clock, its clock transition properties have not been computed accurately. For example, for ^{88}Sr, to the best of our knowledge, there is only one study on the lifetime of the metastable clock state and that too is obtained using a model potential based calculation [31]. Considering that there are no experimental data, fully *ab initio* based calculations, especially using an accurate many-body methods such as relativistic coupled-cluster (RCC), would be crucial to get better insights into the clock transition. Similarly, for ^{87}Sr, the available theoretical data on the lifetime of the clock state are limited to model potential [31], MCDF [32] and CI+MBPT [33] calculations. Moreover, the inclusion of relativistic and QED corrections in the properties calculation is essential to obtain reliable results. It can thus be surmised that there is a clear gap in terms of the availability of accurate properties results for clock transition in Sr.

Considering this, in this work, we employ an all-particle multireference Fock-space relativistic coupled-cluster (FSRCC) theory to investigate the clock transition properties in both Fermionic and Bosonic isotopes of Sr. It should be noted that, RCC theory is one of the most reliable many-body methods for atomic structure calculations, as it accounts for electron correlation to all orders of residual Coulomb interaction. The RCC has been employed to obtain accurate properties results in several closed-shell and one-valence atoms and ions [34–37]. Its application for two-valence atomic systems, is, however, limited to few studies [38–42] due to the complications associated with the implementation of FSRCC theory for multi-reference systems [38–41]. Using the FSRCC theory, we have computed the excitation energies for several low lying states, E1 and M1 transition amplitudes, and hyperfine matrix elements associated with $5s^2\ ^1S_0 \rightarrow 5s5p\ ^3P_0$ clock transition. Further, using these results, we have calculated the lifetimes of the metastable clock states for both ^{87}Sr and ^{88}Sr. In addition, we employ FSRCC theory to calculate the normal mass shift (NMS), specific mass shift (SMS), and field shift (FS) parameters for clock transition $5s^2\ ^1S_0 \rightarrow 5s5p\ ^3P_0$ and two intercombination lines, $5s^2\ ^1S_0 \rightarrow 5s5p\ ^3P_1$ and $5s^2\ ^1S_0 \rightarrow 5s5p\ ^1P_1$, in Sr. Furthermore, we employ a perturbed relativistic coupled-cluster (PRCC) theory [37, 43–46] to calculate the ground state electric dipole polarizability (α) of Sr. It should be noted that, α is a crucial parameter in estimating the blackbody radiation (BBR) shift in the clock transition frequency. The other key merits of our work are: first, to further improve the accuracies of our results, we have incorporated the corrections from the Breit interaction, QED effects, and perturbative triples in our calculations; second, to test the convergence of our results, we have employed large basis sets in the FSRCC and PRCC calculations.

The remainder of the paper is organized into five sections. In Sec. II, we provide a brief description of the FSRCC theory for two-valence atomic systems. We have given the coupled-cluster working equation for two-valence systems. In the same section, we also provide the expressions for hyperfine induced and E1M1 transition rates, and perturbative triples corrections to the energy of two-valence systems. The results obtained from our calculations are presented and discussed in different subsections of Sec. III. Theoretical uncertainty in our computed results is discussed in Sec. IV of the paper. Unless stated otherwise, all results and equations presented in this paper are in atomic units ($\hbar = m_e = e = 1/4\pi\epsilon_0 = 1$).

II. METHODOLOGY

Since the properties of our interest involves atomic state functions (ASFs) of two-valence nature, we need an accurate multireference theory to calculate the many-body wavefunctions and the properties. Considering this, in the present work we have employed an all-particle FSRCC theory for two-valence [40, 41] systems to probe the clock transition and related properties in Sr. In Ref. [47], we have discussed in detail the implementation of FSRCC theory for closed-shell and one-valence systems to a sophisticated parallel code and have given the working equations and the contributing Goldstone diagrams. So, here, for completeness, we provide a very brief description of the FSRCC theory for two-valence systems and the properties calculations in the context of two-valence Sr.

A. Two-valence FSRCC Theory

The atomic state function for a two-valence atom or ion is obtained by solving the many-body Schrodinger equation

$$H^{\rm DCB}|\Psi_{vw}\rangle = E_{vw}|\Psi_{vw}\rangle, \tag{1}$$

where $|\Psi_{vw}\rangle$ is the exact many-body wavefunction and E_{vw} is the corresponding exact energy. The indices $v, w, \cdots$ represent the valence orbitals. $H^{\rm DCB}$ is the Dirac-Coulomb-Breit no-virtual-pair Hamiltonian expressed as

$$\begin{aligned} H^{\rm DCB} &= \sum_{i=1}^{N}\left[c\boldsymbol{\alpha}_i\cdot\mathbf{p}_i + (\beta_i-1)c^2 - V_N(r_i)\right] \\ &\quad + \sum_{i<j}\left[\frac{1}{r_{ij}} + g^{\rm B}(r_{ij})\right], \end{aligned} \tag{2}$$

where $\boldsymbol{\alpha}$ and β are the Dirac matrices, and $1/r_{ij}$ and $g^{\rm B}(r_{ij})$ are the Coulomb and Breit interactions, respectively. In FSRCC theory, $|\Psi_{vw}\rangle$ is written as

$$|\Psi_{vw}\rangle = e^T\left[1 + S_1 + S_2 + \frac{1}{2}\left({S_1}^2 + {S_2}^2\right) + R_2\right]|\Phi_{vw}\rangle, \tag{3}$$

where $|\Phi_{vw}\rangle, = a_w^\dagger a_v^\dagger|\Phi_0\rangle$, is the Dirac-Fock reference state for a two-valence system. Operators T, S and R are the electron excitation operators, referred to as the coupled-cluster (CC) operators, for closed-shell, one-valence and two-valence sectors, respectively. The subscripts 1 and 2 with these operators represent the single and double excitations, referred to

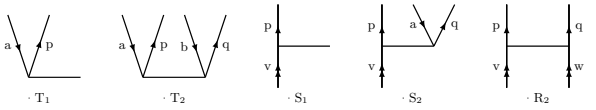

FIG. 1. The diagrammatic representation of closed-shell, one-valence and two-valence single and double CC operators.

as the coupled-cluster with singles and doubles (CCSD) approximation. The FSRCC theory with CCSD approximation subsumes most of the electron correlation effects in atomic properties and provides an accurate description of the calculated properties. In the second quantized representation, these CC operators are expressed as

$$T_1 = \sum_{ap} t_a^p a_p^\dagger a_a \;\text{ and }\; T_2 = \frac{1}{2!}\sum_{abpq} t_{ab}^{pq} a_p^\dagger a_q^\dagger a_b a_a, \quad (4a)$$

$$S_1 = \sum_{p} s_v^p a_p^\dagger a_v \;\text{ and }\; S_2 = \sum_{apq} s_{va}^{pq} a_p^\dagger a_q^\dagger a_a a_v, \quad (4b)$$

$$R_2 = \sum_{pq} r_{vw}^{pq} a_p^\dagger a_q^\dagger a_w a_v. \quad (4c)$$

Here, the indices $a, b, \ldots$ and $p, q, \ldots$ represent the core and virtual orbitals, respectively. And, $t_{\ldots}^{\ldots}$, $s_{\ldots}^{\ldots}$ and $r_{\ldots}^{\ldots}$ are the cluster amplitudes corresponding to T, S and R cluster operators, respectively. The diagrammatic representations of these operators are shown in Fig. 1.

The operators for closed-shell and one-valence sectors are obtained by solving the set of coupled nonlinear equations discussed in Refs. [35] and [48], respectively. The two-valence CC operator, R_2, is obtained by solving the CC equation [40, 41]

$$\langle\Phi_{vw}^{pq}|\bar{H}_{\rm N} + \{\overbrace{\bar{H}_{\rm N}S'}\} + \{\overbrace{\bar{H}_{\rm N}R_2}\}|\Phi_{vw}\rangle = E_{vw}^{\rm att}\langle\Phi_{vw}^{pq}|\Big[S' + R_2\Big]|\Phi_{vw}\rangle. \quad (5)$$

Here, for compact notation we have used $S' = S_1 + S_2 + \frac{1}{2}(S_1^2 + S_2^2)$. $E_{vw}^{\rm att}$ is the two-electron attachment energy and is defined as the difference between the correlated energy of $(n-2)-$electron (closed-shell) and $n-$electron (two-valence) sectors, $E_{vw} - E_0$. And, $\bar{H}_N, = e^{-T^{(0)}} H_N e^{T^{(0)}}$, is a similarity transformed Hamiltonian, which using Wick's theorem, can be reduced to the form

$$\bar{H}_N = H_N + \{\overbrace{H_N T^{(0)}}\} + \frac{1}{2!}\{\overbrace{H_N T^{(0)} T^{(0)}}\} + \frac{1}{3!}\{\overbrace{H_N T^{(0)} T^{(0)} T^{(0)}}\} + \frac{1}{4!}\{\overbrace{H_N T^{(0)} T^{(0)} T^{(0)} T^{(0)}}\} \quad (6)$$

B. Perturbative triples correction to energy

Considering the complicated nature of electron correlations in two-valence systems, it is important to include the correlation effects from triple excitations in FSRCC. In our previous work [41], we have implemented triples corrections to the properties of two-valence systems using perturbative approach. It should be noted that, the perturbative triples incorporate dominant contributions from triple excitations with far less computational cost than full triples. Considering this, in this work, we implement triples corrections to energy using perturbative approach.

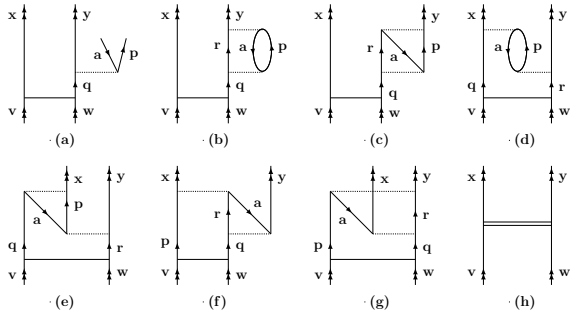

FIG. 2. The Golstone diagrams contributing to perturbative triples $\widetilde{R}_3$ (diagram (a)) and correlation energy (diagrams (b - g)) arising from perturbative triples. Diagram (h) represents a two-body effective operator using which valence-states are coupled to give atomic state functions, as shown in Fig. 3.

Since magnitude of two-valence CC operator R_2 is larger than T and S operators for two-valence systems, for this, we choose the triples which arise from R_2. After a two-body residual interaction, $g_{ij} = \sum_{i<j}[\frac{1}{r_{ij}} + g^{\rm B}(r_{ij})]$, contracted with R_2, it leads to perturbative triples operator, $\widetilde{R}_3 = \overbrace{g R_2}$. The Goldstone diagram corresponding to $\widetilde{R}_3$ is shown in Fig. 2(a), which corresponds to the algebraic expression

$$\widetilde{R}_3 \approx \frac{1}{\Delta\epsilon_{vwa}^{xyp}} a_x^\dagger a_y^\dagger a_p^\dagger a_a a_w a_v \sum_q \langle yp|g|qa\rangle\langle xq|R_2|vw\rangle, \quad (7)$$

where $\Delta\epsilon_{vwa}^{xyp} = \epsilon_v + \epsilon_w + \epsilon_a - \epsilon_x - \epsilon_y - \epsilon_p$. The operator $\widetilde{R}_3$ now contract with residual Coulomb interaction to contribute to the energy. There are *six* energy diagrams from $\widetilde{R}_3$, shown as diagrams (b - g) in Fig. 2. These diagrams correspond to the algebraic expression

$$\begin{aligned}\{\overbrace{g\widetilde{R}_3}\}_{vw}^{xy} &= \sum_{apqr} \frac{1}{\Delta\epsilon_{vwa}^{xrp}} [\tilde{g}_{yarp} g_{rpqa} r_{xqvw} \\ &+ \tilde{g}_{xaqp} g_{pyar} r_{qrvw} - g_{xapr} g_{ryqa} r_{pqvw} \\ &- g_{aypr} g_{xraq} r_{pqvw}], \end{aligned} \quad (8)$$

where $\tilde{g}_{ijkl} = g_{ijkl} - g_{jikl}$. The diagrams (b - g) are computed with respect to uncoupled states and stored in the form an effective diagram, digram (h). Next, we couple the single particle valence orbitals to give the atomic state function. Angular factors arising from this coupling is provided in Fig. 3.

C. Hyperfine induced E1 transition rate

Since Fermionic isotope of Sr possess non zero nuclear spin, the clock transition can be allowed through a hyperfine interaction. The hyperfine state, $|\Gamma F M_F\rangle$, is obtained

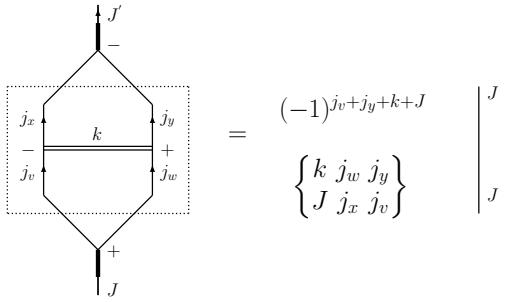

$$= (-1)^{j_v+j_y+k+J} \begin{Bmatrix} k & j_w & j_y \\ J & j_x & j_v \end{Bmatrix}$$

FIG. 3. Angular factors arising from the coupling of single-particle states of a two-body effective energy operator.

by coupling an electronic state with the eigenstate of the nuclear spin operator $\mathbf{I}$. Considering the hyperfine interaction Hamiltonian, $H_{\rm HFS}$, as a perturbation, we can write, within the first-order time-independent perturbation theory,

$$|\Gamma F M_F\rangle = \sum_n \left[\frac{\langle\gamma_n\Psi_n\gamma_I I|H_{HFS}|\gamma_0\Psi_0\gamma_I I\rangle}{E_0-E_n}\right]\times|\gamma_n\Psi_n\gamma_I I\rangle. \quad (9)$$

The term within the bracket represents the hyperfine mixing of unperturbed state $|\gamma_0\Psi_0\gamma_I I\rangle$ with an excited state $|\gamma_n\Psi_n\gamma_I I\rangle$. The parameters Γ and γ_i are additional quantum numbers to identify the states uniquely, and E is the exact energy.

The transition rate between two hyperfine levels $|\Gamma_i F_i M_{F_i}\rangle$ and $|\Gamma_f F_f M_{F_f}\rangle$ is expressed as [49]

$$\Gamma_{\rm HFS} = \frac{4\alpha\omega^3}{3c^2}\frac{1}{(2F_i+1)}|E1_{\rm HFS}|^2, \quad (10)$$

where α is the fine structure constant, c is the speed of light, and ω is the transition frequency. $E1_{\rm HFS}$ is referred to as the HFS induced electric dipole transition amplitude and, using the expressions for dipole and hyperfine matrix elements [49, 50], can be derived to the form

$$E1_{\rm HFS} = c(I,J,F,\mu_I)\left[\frac{\langle\Psi_f||\mathbf{t}^1||\bar{\Psi}_n\rangle\langle\bar{\Psi}_n||\mathbf{d}||\Psi_i\rangle}{E_{\bar{n}}-E_i} + \frac{\langle\Psi_f||\mathbf{d}||\Psi_n\rangle\langle\Psi_n||\mathbf{t}^1||\Psi_i\rangle}{E_n-E_i}\right], \quad (11)$$

where c(I, J, F, μ_I) is the angular factor associated with the coupling of nuclear and electronic angular states. Here, $\mathbf{d}$ is the dipole operator and $\mathbf{t}^1$ is the magnetic dipole hyperfine operator [49, 51]. As evident from Eq. (11), clock transition in Fermionic Sr can occur in two pathways. First, the initial state couples to the opposite parity intermediate states via a dipole transition, and then transitions to clock state via a hyperfine interaction. Alternatively, the initial state can couple to the same parity intermediate states through a hyperfine interaction and then connect to clock state through a dipole operator. For the present case of ^{87}Sr: $|\Psi_i\rangle = 5s^2\,{}^1S_0$, $|\Psi_f\rangle = 5s5p\,{}^3P_0^o$, $|\bar{\Psi}_n\rangle = 5s5p\,{}^3P_1^o$, $5s5p\,{}^1P_1^o$, $5s6p\,{}^3P_1^o$, $5s6p\,{}^1P_1^o$, and $|\Psi_n\rangle = 5s6s\,{}^3S_1$, $5s4d\,{}^3D_1$.

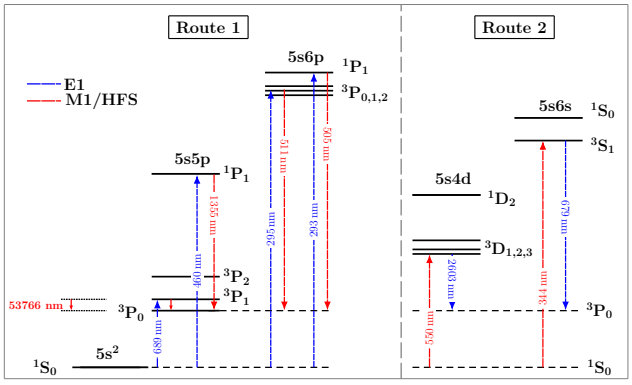

FIG. 4. Schematic energy level diagram showing the $5s^2\,{}^1S_0 - 5s5p\,{}^3P_0^o$ clock transition in ^{87}Sr and ^{88}Sr via a HFS induced and a two-photon E1+M1 channel, respectively.

D. E1M1 transition rate

In Bosonic isotopes of Sr, since they possess a zero nuclear spin, the clock transition can occur via a *two-photon* E1 + M1 transition. Like the case of Fermionic Sr, it can happen in two pathways. In the first, the initial state $|\Psi_i\rangle$ couples to opposite parity intermediate states $|\bar{\Psi}_n\rangle$ via an electric dipole transition, and then decays to final state $|\Psi_f\rangle$ through a magnetic dipole transition (emitting a photon of energy ω_1). And in the second pathway, the initial state couples with same parity intermediate states $|\Psi_n\rangle$ via a magnetic dipole operator (emitting a photon of energy ω_2), then connects to final state through an electric dipole transition. Mathematically, the E1+M1 transition rate between $|\Psi_i\rangle$ and $|\Psi_f\rangle$ can be expressed in terms of the reduced matrix elements of the E1 and M1 operators, as [31, 42]

$$\Gamma_{E1M1} = \frac{8}{27\pi}\alpha^6\int_0^\infty d\omega_1\omega_1^3\int_0^\infty d\omega_2\omega_2^3\,|E1_{\rm M1}|^2, \quad (12)$$

where E1+M1 transiton amplitude is expressed as

$$E1_{\rm M1} = \left[\frac{\langle\Psi_f||m_1||\bar{\Psi}_n\rangle\langle\bar{\Psi}_n||\mathbf{d}||\Psi_i\rangle}{E_{\bar{n}}+\omega_1-E_i} + \frac{\langle\Psi_f||\mathbf{d}||\Psi_n\rangle\langle\Psi_n||m_1||\Psi_i\rangle}{E_n+\omega_2-E_i}\right] \times\delta(E_i+\omega_1+\omega_2-E_f). \quad (13)$$

Here, since the transition is allowed through a two photon channel, the energy difference of final and initial states satisfies $E_f - E_i = \omega_1 + \omega_2$.

The reduced matrix elements in Eqs. (11) and (13) are calculated using FSRCC theory. The details related to the calculation is provided in our previous works [40, 41].

E. Isotope Shift

Isotope shifts in energy of an atom or ion arise from the variations in nuclear mass and charge distributions between

two isotopes. Incorporating isotope shifts in the calculations of atomic properties has become important due to the pressing need to match atomic theory calculations with high accuracy atomic experiments. The isotope shifts in energy of a two-valence atom or ion within the framework of multireference coupled-cluster theory can be calculated as

$$\Delta E_{\rm iso} = \frac{\langle \Psi_{vw} | H_{\rm iso} | \Psi_{vw} \rangle}{\langle \Psi_{vw} | \Psi_{vw} \rangle}, \tag{14}$$

where $|\Psi_{vw}\rangle$ is an exact atomic state function obtained by solving Eq. (1) using multireference FSRCC theory, and operator $H_{\rm iso}$ is an isotope shift Hamiltonian. $H_{\rm iso}$ embeds two important contributions: the field shift ($H_{\rm FS}$), which arises due to varying nuclear charge distribution between two isotopes; and the mass-shift ($H_{\rm MS}$), which occurs due to recoil motion of the nucleus. The mass-shift Hamiltonian can further be separated to have two contributions, $H_{\rm MS} = H_{\rm NMS} + H_{\rm SMS}$, where $H_{\rm NMS}$ and $H_{\rm SMS}$ are referred to as the normal mass-shift and specific mass shift operators, respectively. The $H_{\rm NMS}$ is a one-body operator, and expressed as [52, 53]

$$H_{\rm NMS} = \frac{1}{2M}\sum_{i=1}^{N} \Big[\mathbf{p}_i^2 - \frac{\alpha Z}{r_i}\big((\alpha_i \cdot \mathbf{p}_i) - (\alpha_i \cdot \mathbf{C}_i^1)(\mathbf{C}_i^1 \cdot \mathbf{p}_i)\big)\Big], \tag{15}$$

where M is the nuclear mass, α_i is the Dirac matrix, α is the fine structure constant, Z is the atomic number, and $\mathbf{p}_i$ and $\mathbf{C}^1$ are the momentum and Racah operators, respectively. The specific mass-shift operator $H_{\rm SMS}$, on the other hand, is a two-body operator, and expressed as [52, 53]

$$H_{\rm SMS} = \frac{1}{M}\sum_{i<j}^{N} \Big[\mathbf{p}_i \cdot \mathbf{p}_j - \frac{\alpha Z}{r_i}\big((\alpha_i \cdot \mathbf{p}_j) - (\alpha_i \cdot \mathbf{C}_i^1)(\mathbf{C}_i^1 \cdot \mathbf{p}_j)\big)\Big], \tag{16}$$

Considering the nucleus as a uniformly charged sphere of radius R, the field-shift Hamiltonian $H_{\rm FS}$ represents the modification in the nuclear potential experienced by an electron due to a small change δR in the nuclear charge radius. This perturbation accounts for the variation in the electronic energy arising from differences in the nuclear charge distribution between isotopes and, therefore, is responsible for the field (or volume) contribution to the isotope shift. The corresponding Hamiltonian can be expressed [49]

$$H_{\rm FS} = \begin{cases} -\frac{5Z}{4R^3}\left[1 - r^2/R^2\right] \text{ for } r \le R \\ 0 \text{ for } r > R. \end{cases} \tag{17}$$

The details, such as one- and two-body operators' matrix elements, contributing Goldstone diagrams to Eq. (14), algebraic expressions and angular factors, etc., related to the implementation of isotope shifts calculations for one- and two-valence systems within the framework of FSRCC theory shall be provided in a separate work [54].

TABLE I. Comparison of single-particle and SCF energies (in hartree) from GTO with GRASP2K and B-Spline results. The optimized parameters, α_0 and β, for the even-tempered basis used in our calculations are also included.

Orbitals	GTO	GRASP2K	B-Spline
$1s_{1/2}$	−596.12431	−596.12414	−596.12464
$2s_{1/2}$	−83.64336	−83.64329	−83.64334
$2p_{1/2}$	−75.87558	−75.87551	−75.87553
$2p_{3/2}$	−73.34196	−73.34194	−73.34194
$3s_{1/2}$	−14.45568	−14.45567	−14.45568
$3p_{1/2}$	−11.57593	−11.57592	−11.57592
$3p_{3/2}$	−11.17082	−11.17081	−11.17082
$3d_{3/2}$	−6.12644	−6.12645	−6.12643
$3d_{5/2}$	−6.05602	−6.05602	−6.05601
$4s_{1/2}$	−2.43444	−2.43445	−2.43444
$4p_{1/2}$	−1.61374	−1.61374	−1.61374
$4p_{3/2}$	−1.56683	−1.56683	−1.56683
$E_{\rm SCF}$	−3177.52169	−3177.52166	−3177.52251
Parameter	s	p	d
α_0	0.00539	0.00567	0.00494
β	1.995	1.982	2.045

III. RESULTS AND DISCUSSIONS

A. Single-particle basis and convergence of properties

Accurate single-particle basis is essential to get reliable results using FSRCC and PRCC theories. In this work, we have employed Gaussian-type orbitals (GTOs) [55] as the single-electron basis. GTOs form a finite basis set where single-particle wavefunctions are expressed as linear combinations of Gaussian-type functions (GTFs). The large component of the wavefunction is expressed as

$$g^L_{\kappa p}(r) = C^L_{\kappa i} r^{n_\kappa} e^{-\alpha_p r^2}, \tag{18}$$

where $p = 0, 1, 2, \ldots, N$ refers to the GTO index and N is the total number of GTFs. The exponent α_p is further expressed as $\alpha_0 \beta^{p-1}$, where α_0 and β are two independent parameters. Parameters α_0 and β are optimized separately for each orbital symmetry to ensure that the single-electron wavefunctions and energies match well with the numerical values obtained from GRASP2K [56]. The small components of the wavefunctions are derived from the large components by applying the kinetic balance condition [57].

In Table I, we list the values of optimized α_0 and β parameters along with the single-particle and self-consistent-field (SCF) energies for Sr. For comparison, we have also provided the results from GRASP2K [56] and B-spline [58] calculations. The single-electron basis used in our calculations also incorporate the effects of vacuum polarization and self-energy corrections. As evident from the table, both single-particle as well as SCF energies from GTO show an excellent agreement with GRASP2K and B-spline results. The maximum differences are observed to be 0.00003% and 0.00006% for SCF and single-particle energies, respectively.

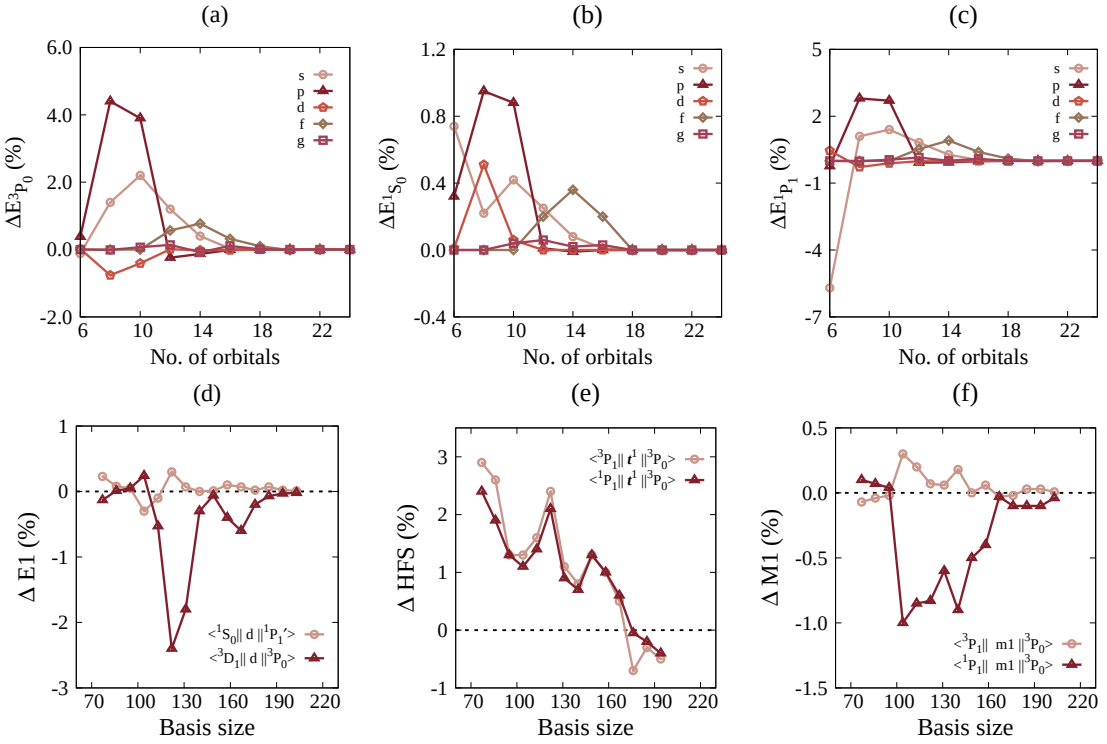

FIG. 5. Panels (a - c) show the convergence trend for energy of $^3P_0$, $^1S_0$ and $^1P_1$ states with augmentation of orbitals in s, p, d, f and g symmetries. Panels (d - f) show the convergence trend for E1, HFS, and M1 reduced matrix elements with basis size.

Since GTOs form a mathematically incomplete basis, it is essential to check the convergence of the properties with basis size. Panels (a - c) of Fig. 5 show the percentage change in the excitation energies for $^3P_0$, $^1S_0$ and $^1P_1$ states, respectively, as a function of number of orbitals in s, p, d, f, and g symmetries. As can be expected, lower energy orbitals in each symmetry show a stronger electron correlation effect. The contribution to energy decreases with an increase in the number of orbitals in each symmetry. For $^3P_0$ and $^1S_0$ states, the dominant electron correlation is observed from s, p, d and f-electrons, whereas for $^1P_1$ state, it is from s, p and f-electrons. From a systematic analysis of calculations, we find that the energies converge well with $19s$, $17p$, $17d$, $14f$, and $8g$ orbitals, yielding a total basis size of 131. We also checked the contributions from the orbitals from h-symmetry and higher, however, their contributions to energy were found to be negligible. Similarly, to check the convergence of the properties, we calculated E1, HFS and M1 matrix elements as a function of basis size. As evident from the Table IX, we begin with a moderate size basis of 68 orbitals and systematically add orbitals in each symmetry until the change in the property becomes negligible. Panels (d - f) show the percentage change as a function of basis size for some key E1, HFS and M1 matrix elements as an example. As discernible from the figures, all the three properties converge well with basis size. Other key point to note is that, properties require larger basis to converge than energy.

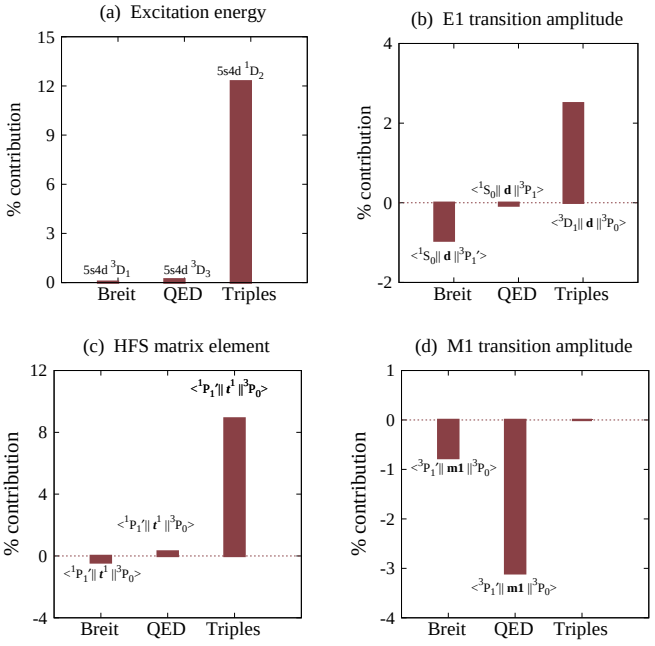

FIG. 6. Dominant percentage contributions from the Breit interaction, QED effects and perturbative triples to excitation energy (panel (a)), E1 transition amplitudes (panel (b)), HFS matrix elements (panel (c)), and M1 transition amplitudes (panel (d)) for Sr.

TABLE II. Two-electron removal energy for $^1S_0$ state (cm^{-1}) and excitation energies for some low-lying even- and odd-parity excited states of Sr. The results listed correspond to $5s^2$, $5s5p$, $5s4d$, $5s6s$, $5s6p$ configurations in the model space. For quantitative analysis of electron correlations, contributions from the Breit interaction, QED corrections and perturbative triples are listed separately.

States	DC-CCSD	Breit	Self-energy	Vac-pol	Triples	Total	Other cal.	NIST[59]	% Error
$5s^2\ ^1S_0$	135785	0	0	4	238	136027	136244[b], 135444[c], 135940[f]	134897[a]	0.84
$5s5p\ ^3P_0$	14901	4	0	6	−393	14518	14241[d], 14806[b], 14550[c] 12490[e], 14860[f]	14318[a]	1.4
$5s5p\ ^3P_1$	15176	3	0	6	−387	14798	14995[b], 14739[c], 14448[d] 12663[e], 14854[f]	14504[a]	2
$5s5p\ ^3P_2$	15720	0	0	6	−382	15344	15399[b], 15142[c], 14825[d] 13022[e], 14783[f]	14899[a]	2.9
$5s4d\ ^3D_1$	19840	−10	0	−25	−1719	18086	18255[b], 18327[c], 18076[d] 19571[e], 18409[f]	18159[a]	−0.4
$5s4d\ ^3D_2$	19859	−10	0	−29	−1722	18098	18298[b], 18394[c], 18141[d] 19587[e], 18569[f]	18218[a]	−0.6
$5s4d\ ^3D_3$	19906	−12	0	−37	−1719	18138	18422[b], 18506[c], 18254[d] 19617[e], 18747[f]	18319[a]	−0.9
$5s4d\ ^1D_2$	22026	−9	0	−24	−2406	19587	20428[b], 20441[c], 19968[d] 20166[e], 20509[f]	20149[a]	−2.8
$5s5p\ ^1P_1$	22834	1	0	5	−505	22335	21955[b], 21823[c], 21469[d] 20832[e], 23387[f]	21698[a]	2.9
$5s6s\ ^3S_1$	30375	1	0	5	−242	30139	29369[b], 29223[c] 29019[d], 27488[e]	29038[a]	3.8
$5s6s\ ^1S_0$	32292	1	0	5	−1045	31253	30938[b], 30777[c]	30591[a]	2.2
$5s6p\ ^3P_0$	35747	1	0	6	−321	35433	34241[b], 34055[c]	33853[a]	4.7
$5s6p\ ^3P_1$	35803	1	0	6	−791	35019	34255[b], 34071[c] 33814[d], 32110[e]	33868[a]	3.4
$5s6p\ ^3P_2$	35939	0	0	6	−316	35629	34365[b], 34134[c]	33973[a]	4.9
$5s6p\ ^1P_1$	36256	0	0	7	−750	35513	34476[b], 34308[c], 34105[d] 32487[e]	34098[a]	4.1

[a] Ref. [59] - Expt. , [b] Ref. [60] - CI + MBPT, [c] Ref. [60] - CI + all-order, [d] Ref. [61] - CI + MBPT , [e] Ref. [61] - CI, [f] Ref. [62] - FSRCC.

B. Excitation Energy

In Table II, we present the excitation energies for several low lying states of Sr from FSRCC calculation. The excitation energy of a general state $nln'l'\ ^{(2S+1)}L_J$ can be calculated as

$$\Delta E_{nln'l'\ ^{(2S+1)}L_J} = E_{nln'l'\ ^{(2S+1)}L_J} - E_{ns^2\ ^1S_0}, \qquad (19)$$

where $E_{ns^2\ ^1S_0}$ and $E_{nln'l'\ ^{(2S+1)}L_J}$ are the exact energies of the ground and excited states, respectively. In Table II, we have also provided the experimental energies and the results from other theory calculations for comparison. To improve the accuracy of our energies, we have incorporated the corrections the from Breit interaction and QED effects in our calculations. The other two important points to note in our study are, the inclusion of high energy configurations in the model space and the corrections from the perturbative triples. High energy configurations are essential to incorporate in multireference systems to account for *valence-valence* electron correlation accurately. In this work, we include $5s4d$, $5s6s$, and $5s6p$ high energy configurations in model space, in addition to the bare even and odd parity configurations $5s^2$ and $5s5p$, respectively. It is to be mentioned that, while two-valence FSRCC calculations with extended model spaces are quite challenging due to *intruder* states problem, we observed significant reductions to the errors in the energies. Similarly, perturbative triples are observed improve the energies significantly. Fig. 6(a) shows the largest percentage contributions from Breit, QED and perturbative triples corrections to the energy. The largest contribution from perturbative triples is found to be $\approx 12\%$ in the case of 5s4d $^1D_2$ state. Whereas, the Breit and cumulative QED corrections are observed to ≈ 0.1 and 0.2%, respectively, in the case of 5s4d$^3D_1$ and 5s4d$^3D_3$ states.

Table II also shows the relative errors in our excitation energies with respect to NIST data. As evident, despite our efforts to improve energies by incorporating different corrections and high energy configurations, we get a large variation in the errors. The smallest and largest errors in our calculations are 0.4 and 4.9%, respectively, in the case of 5s4d$^3D_1$ and 5s6p$^3P_2$ states. Unlike the case of one-valence atoms or ions, large errors in the *ab initio* calculations of multireference systems are anticipated due to the complicated nature of electron correlations. Typically, there are three types of electron correlations exhibited by a multireference atom or ion; *core-core*, *core-valence* and *valence-valence*. It is extremely challenging to treat all these three accurately to the same level within the framework of a single theory. In the present work,

within the framework of a FSRCC theory, *core-core* and *core-valence* correlations are accounted to all orders of residual Coulomb interaction using a nonlinear RCC theory. And, the *valence-valence* correlation is treated in the framework of CI through an effective Hamiltonian approach. Looking into the literature, to the best of our search, we could find three previous works which report excitation energies for two-valence Sr [60–62]. Ref. [60] uses CI+MBPT and CI+all-order method, whereas Ref. [61] has employed CI+MBPT and CI methods to compute excitation energies. The third calculation [62] is using the same method as the present work, however, with some key additions in the present work. Consistent with the trends in our calculations, the previous calculations also show large errors. For example, consider the case of metastable clock state 5s5p$^3P_0$, which is of the primary interest of our work, the errors in excitation energy are $\approx 3.4\%$ CI+MBPT [60], 1.6% CI+all-order [60], 0.5% CI+MBPT [61], 12.8% CI [61], and 3.8% FSRCC [62]. The error in the present calculation is $\approx 1.4\%$. The reason for the difference in the excitation energy from Ref. [62] could be attributed to the inclusion of the contributions from *nonlinear* terms in FSRCC, high energy configurations, and Breit and QED corrections in the present work.

C. E1, HFS and M1 Reduced Matrix Elements

In Table III, we present our results on E1, HFS and M1 reduced matrix elements from FSRCC calculations. These reduced matrix elements, along with the energies, are required to calculate the lifetime of the metastable clock state. To improve the accuracy of these matrix elements, we have incorporated the corrections from relativistic and QED effects, and also from the perturbative triples in our calculations. It is to be also mentioned that, the results presented in the table correspond to a larger model space with $5s^2$, $5s5p$, $5s4d$, $5s6s$, $5s6p$ configurations.

As evident from the table, and as can be expected, DF has the dominant contributions for all the matrix elements. To give an example from each category of reduced matrix elements, it contributes $\approx 95\%$, 97%, and 117% of the total value for $\langle {}^1S_0||\mathbf{d}||{}^1P_1\rangle$, $\langle {}^3P_1||t^1||{}^3P_0\rangle$ and $\langle {}^3P_1||m1||{}^3P_0\rangle$ matrix elements. The next dominant contributions come from the electron correlations due to residual Coulomb interaction. It contributes $\approx 4.6\%$, 2.0%, and -16.5%, respectively, to these reduced matrix elements. As discernible from Fig. 6, Breit, QED and perturbative triples too have the significant contributions. The largest contribution from the Breit is observed to be $\approx 1.0\%$ in the case of $\langle {}^1S_0||\mathbf{d}||{}^3P_1'\rangle$, whereas a maximum QED correction of $\approx -3.1\%$ is observed in the case of $\langle {}^3P_1'||m1||{}^3P_0\rangle$ reduced matrix elements. Perturbative triples are observed to have a large contribution of $\approx 8.9\%$ in the case of $\langle {}^1P_1'||t^1||{}^3P_0\rangle$.

As can be observed from the table, there are several other theoretical and experimental studies on E1 reduced matrix elements in literature. The other theoretical values reported are using the methods like CI, MBPT, CI+MBPT, CI+all-order and different variations of MCDF. Among all these methods, in terms of accurate treatment of electron correlations, CI+all-order is closest to ours. There is, however, a key difference that it accounts for *core-core* and *core-valence* correlations only to the level of linear terms in CC. In FSRCC, however, we consider the nonlinear terms as well, which is crucial for multireference systems. For a comparative analysis, we consider the reduced matrix element $\langle {}^1S_0||\mathbf{d}||{}^1P_1\rangle$, which is expected to have a dominant contribution to the lifetime of the clock state. We notice a significant variation in the values reported from previous theory calculations and experiments for this. For example, the smallest value obtained using CI+CMP [65] defer by $\approx 10\%$ with the largest reported value using MCDF calculation [75]. Similarly, from experiments, there is a difference of $\approx 7\%$ between smallest [68] and largest [79] reported values. Our calculated value, 4.88, is smallest among all the calculations, however, with more closer to the CI+all-order value [60, 66]. However, as evident from Table IV where we provide configuration-wise matrix elements, the reason for a smaller value is attributed to the more accurate treatment of *valence-valence* electron correlation, with the inclusion of higher energy configurations in the model space. Our value, 4.99, with bare configurations $5s^2$ and $5s5p$ compares well with calculations [60, 66], and in general with others, with a small difference due to relativistic, QED and perturbative triples corrections in our result. A similar trend of comparison and analysis also apply to all other E1 reduced matrix elements where our results are within the range of previous calculations and experiments, except for $\langle {}^1S_0||\mathbf{d}||{}^1P_1'\rangle$ where our E1 amplitude is an order more than previous calculations.

To compare our results for HFS reduced matrix elements, to the best of our knowledge, we could find only one previous calculation [32]. Ref. [32] reports HFS reduced matrix elements for ${}^3P_1 \rightarrow {}^3P_0$ and ${}^1P_1 \rightarrow {}^3P_0$ transitions using MCDHF calculation. Our computed reduced matrix elements are larger by ≈ 42 and 31%, respectively, with respect to Ref. [32]. The reason for this is attributed to an accurate treatment of electron correlation effects in FSRCC theory. It should be noted that, MCDF suffers from an inherent dependency on the choice of configurations to incorporate the electron correlation effects, and therefore, does not provide an accurate treatment of *core-core* and *core-valence* correlations. The cumulative contributions from Breit and QED corrections from Ref. [32] are 0.35 and 0.41%, respectively to the total value for the two transitions. We observed a slightly smaller contribution of $\approx 0.2\%$ for each reduced matrix elements.

For M1 reduced matrix elements, to the best of our knowledge, there is only one previous calculation [78]. Ref. [78] reports M1 transition rates for ${}^3P_1 \rightarrow {}^3P_0$ and ${}^1P_1 \rightarrow {}^3P_0$ transitions using MCDF calculation. Our computed M1 reduced matrix element for ${}^3P_1 \rightarrow {}^3P_0$ is $\approx 17\%$ smaller than Ref. [78]. Similarly, we observed a very large difference of $\approx 85\%$ for ${}^1P_1 \rightarrow {}^3P_0$ transition. Again, the reason for these differences could be attributed to inherent limitations with MCDF methods for accounting the electron correlations accurately in many-body calculations.

TABLE III. E1, HFS and M1 reduced matrix elements (in a.u.) for Sr with $5s^2$, $5s5p$, $5s4d$, $5s6s$, $5s6p$ configurations in the model space. The data from experiments and other theory calculations are also provided for comparison (only magnitude).

States	DF	DC-CCSD	Breit	QED	Breit + QED	Triples	Total	Other cal.	Expt.
E1 Reduced Matrix Elements									
$\langle {}^1S_0\|\|\mathbf{d}\|\|{}^3P_1\rangle$	0.1325	0.1404	−0.0011	−0.0001	−0.0012	0.0025	0.1417	0.160[a], 0.158[b] 0.13[e], 0.151[f] 0.1311[i], 0.16[j] 0.152[l]	0.1555[c], 0.1510[d] 0.1486[g], 0.151[h] 0.146[k]
$\langle {}^1S_0\|\|\mathbf{d}\|\|{}^1P_1\rangle$	4.6694	4.8934	0.0	−0.0005	−0.0005	−0.0124	4.8805	5.28[a], 5.272[b] 5.15[e], 5.248[f] 5.298[n], 5.673[o] 5.367[i], 5.292[p] 5.307[l]	5.57[t], 5.40[k] 5.248[h], 5.269[m]
$\langle {}^1S_0\|\|\mathbf{d}\|\|{}^3P_1'\rangle$	0.1308	0.3384	−0.0033	−0.0002	−0.0035	−0.0025	0.3324		
$\langle {}^1S_0\|\|\mathbf{d}\|\|{}^1P_1'\rangle$	−1.2695	−2.6213	−0.0005	−0.0001	−0.0006	0.0314	−2.5905	0.281[b], 0.236[a]	0.26[k]
$\langle {}^3S_1\|\|\mathbf{d}\|\|{}^3P_0\rangle$	2.1231	1.9686	0.0	0.0002	0.0002	0.0046	1.9734	1.96[a], 1.962[b]	2.03[u]
$\langle {}^3D_1\|\|\mathbf{d}\|\|{}^3P_0\rangle$	−2.6236	−2.4329	−0.0002	0.0001	−0.0001	−0.0627	−2.4957	2.74[a], 2.675[b]	2.5[v], 2.7[w]
HFS Reduced Matrix Elements ($\times 10^{-7}$)									
$\langle {}^3P_1\|\|t^1\|\|{}^3P_0\rangle$	2.7867	2.8449	−0.0006	0.0046	0.0040	0.0290	2.8779	2.023[r]	
$\langle {}^1P_1\|\|t^1\|\|{}^3P_0\rangle$	1.9675	2.0534	0.0003	0.0030	0.0033	0.0356	2.0923	1.450[r]	
$\langle {}^3P_1'\|\|t^1\|\|{}^3P_0\rangle$	0.0122	−0.7961	−0.0004	0.0001	−0.0003	0.0149	−0.7815		
$\langle {}^1P_1'\|\|t^1\|\|{}^3P_0\rangle$	−0.5276	−0.1885	0.0009	−0.0006	0.0003	−0.0185	−0.2067		
$\langle {}^1S_0\|\|t^1\|\|{}^3S_1\rangle$	2.5679	2.1257	0.0	0.0024	0.0024	0.0042	2.1323		
$\langle {}^1S_0\|\|t^1\|\|{}^3D_1\rangle$	0.0002	−0.1567	−0.0004	0.0	−0.0004	0.0012	−0.1559		
M1 Reduced Matrix Elements									
$\langle {}^3P_1\|\|m1\|\|{}^3P_0\rangle$	−1.4131	−1.2127	0.0001	−0.0006	−0.0005	0.0	−1.2132	1.413[s]	
$\langle {}^1P_1\|\|m1\|\|{}^3P_0\rangle$	0.0382	0.2684	−0.0002	−0.0005	−0.0007	0.0	0.2677	0.042[s]	
$\langle {}^3P\prime_1\|\|m1\|\|{}^3P_0\rangle$	−0.1929	0.0270	−0.0002	−0.0008	−0.0010	0.0	0.0260		
$\langle {}^1P_1'\|\|m1\|\|{}^3P_0\rangle$	−0.0451	−0.2524	−0.0001	0.0004	−0.0003	0.0	−0.2527		
$\langle {}^1S_0\|\|m1\|\|{}^3S_1\rangle$	0.0	−0.4584	0.0005	0.0060	0.0065	0.0	−0.4519		
$\langle {}^1S_0\|\|m1\|\|{}^3D_1\rangle$	0.0	−0.0002	0.0	0.0	0.0	0.0	-0.0002		

[a] Ref. [61]- CI+MBPT , [b] Ref. [60]- CI+all-order, [c] Ref. [63], [d] Ref. [64], [e] Ref. [65]- CI+CPMP, [f] Ref. [66]- CI+all-order, [g] Ref. [67], [h] Ref. [68], [i] Ref. [69] - CIDF, [j] Ref. [70] - MBPT, [k] Ref. [71] [l] Ref. [72]- DFCP+RCI, [m] Ref. [73], [n] Ref. [74] - CICP, [o] Ref. [75] - MCHF, [p] Ref. [76] - MBPT, [q] Ref. [77]- CI+MBPT, [r] Ref. [32]- MCDHF, [s] Ref. [78]- MCDF, [t] Ref. [79], [u] Ref. [80], [v] Ref. [81], [w] Ref. [82],

TABLE IV. E1, HFS and M1 reduced matrix elements (in a.u.) with increasing energy configurations in the model space. HFS reduced matrix elements are in terms of a factor of 10^{-7}.

Transition	CF1[a]	CF2[b]	CF3[c]	CF4[d]
$\langle {}^1S_0\|\|\mathbf{d}\|\|{}^3P_1\rangle$	0.1033	0.1169	0.1059	0.1404
$\langle {}^1S_0\|\|\mathbf{d}\|\|{}^1P_1\rangle$	4.9905	4.9892	4.5568	4.8934
$\langle {}^3P_1\|\|t^1\|\|{}^3P_0\rangle$	2.4411	2.5027	2.5056	2.8449
$\langle {}^1P_1\|\|t^1\|\|{}^3P_0\rangle$	2.0129	2.0367	2.0328	2.0534
$\langle {}^3P_1\|\|m1\|\|{}^3P_0\rangle$	−1.2308	−1.2321	−1.2134	−1.2127
$\langle {}^1P_1\|\|m1\|\|{}^3P_0\rangle$	0.2897	0.2909	0.2889	0.2684

[a] CF1: $5s^2 + 5s5p$
[b] CF2: $5s^2 + 5s5p + 5s4d$
[c] CF3: $5s^2 + 5s5p + 5s4d + 5s6s$
[d] CF4: $5s^2 + 5s5p + 5s4d + 5s6s + 5s6p$

D. Lifetime of Clock State

Next, we present and discuss our results on the lifetime (τ) of the clock state for Fermionic and Bosonic Sr using FSRCC theory. The τ from our calculations, along with other theory and experimental results, are provided in Table V. As evident from the table, to assess the impact of *valence-valence* electron correlation, we have provided the configuration-wise contributions to lifetime. Moreover, for the same purpose, contributions from the Breit interaction, QED effects and perturbative triples are also listed separately.

1. ^{87}***Sr***

Lifetime of the clock state of ^{87}Sr is calculated as the inverse of the HFS induced transition rate expressed in Eq.(10). For this, we used the E1 and HFS reduced matrix elements from our calculations listed in Table III and experimental en-

TABLE V. Lifetime of the clock state, $5s5p\ ^3P_0^o$, for ^{87}Sr and ^{88}Sr using FSRCC theory. Contributions from the Breit interaction, QED effects, and perturbative triples are provided separately for the quantitative assessment of the electron correlations.

Conf./Methods	τ (s)	
	^{87}Sr	^{88}Sr ($\times 10^9$)
MS1	292.99	2.918
MS2	162.99	2.568
MS3	152.29	2.918
MS4	149.74	9.283
Total CCSD	149.74	9.283
CCSD(T)	143.23	10.200
CCSD(T)+Breit	144.58	9.760
CCSD(T)+Breit+QED	144.25	11.046
Reco.	144.25	11.046
Oth. th.	110(30)[a], 156(9)[b], 132[c], 145(40)[d]	181.82[a]
Expt.	118(3)[e], 330(140)[f], 167^{+79}_{-40}[g], 151.4(48)[h]	

[a] Ref. [31]- Model potential, [b] Ref. [32]- MCDF, [c] Ref. [33]- CI + MBPT, [d] Ref. [83]- Modified Breit-Wills theory, [e] Ref. [84]- Expt., [f] Ref. [85]- Expt., [g] Ref. [86]- Expt., [h] Ref. [87]- Expt.

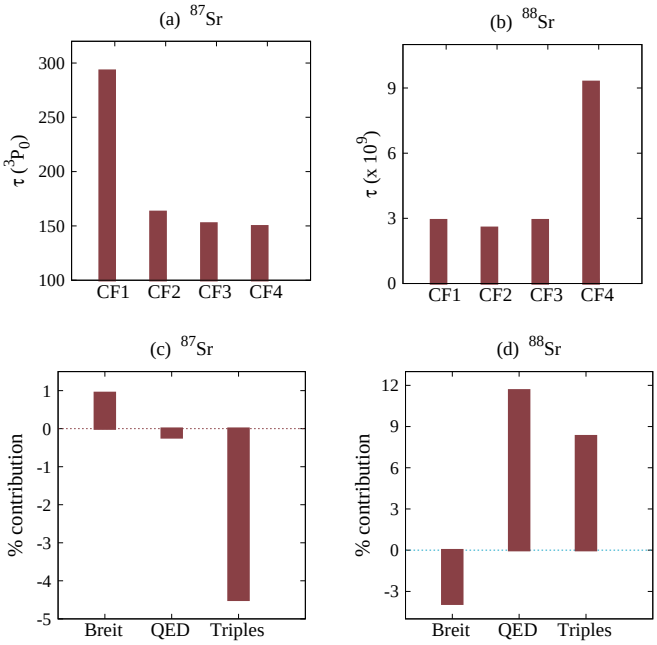

FIG. 7. Percentage cumulative contributions to the lifetime of the clock state from (a), (b) different high energy configurations in model space for ^{87}Sr and ^{88}Sr, respectively. (c), (d) Breit interaction, QED effects and perturbative triples to the lifetime of clock state for ^{87}Sr and ^{88}Sr, respectively.

ergies from the NIST database. Fig 7 shows the cumulative percentage contributions from increasing model space, Breit and QED effects, and perturbative triples to the lifetime. As discernible from the panel (a) of the figure, there is a significant change in τ with the inclusion of high energy configurations. We observed a large change of $\approx$ 49% when the model space is augmented from bare configuration MS1 to an extended configuration MS4. This highlights the importance of *valence-valence* electron correlations in multireference systems. The other significant contribution is from the perturbative triples. We observed a contribution of more than 4% to τ with respect to CCSD value (panel (c)). The cumulative contribution from Breit and QED is observed to be $\approx$ 1% of the total τ (panel (c)).

To compare our result with other theory calculations, we could find four results on τ of ^{87}Sr. None of these are, however, using accurate methods like RCC. The other key point to observe is that, there is a significant variation in the τ reported in these calculations. For example, the smallest reported τ using model potential [31] is smaller by $\approx$30% than the largest reported value using MCDF calculation [32]. The reported τ using CI+MBPT [33] and Modified Breit-Wills theory [83] are in between these two calculations. Moreover, as can be expected due to the nature of many-body methods employed, there are large errors in these calculations. A similar trend of significant variation and large errors is also observed in the experimental values. The reported values are in the range of 118 to 330 s, with a largest error of 47% in recent experiment [86]. Our calculated τ is within the error bars of previous theory and experimental values, and more closer to the CI+MBPT and Modified Breit-Wills theory calculations.

2. ^{88}Sr

The lifetime of the clock state of ^{88}Sr is calculated using E1 and M1 reduced matrix elements from our calculations, provided in Table III, and excitation energies from NIST database in Eq. (12). As discernible from the panel (b) of the Fig. 7, unlike the case of ^{87}Sr, here we observed a different trend of *valence-valence* electron correlation where MS4 is observed to have the largest change of $\approx$ 218% with respect to MS3. The reason for this could be attributed to a strong mixing of $5s6p$ valence configuration with bare configuration $5s5p$. Consistent with ^{87}Sr, but a larger contribution of $\approx$ 10% of the CCSD value was observed from the perturbative triples. Similarly, Breit and QED effects are observed to contribute more. The Breit contribution is $\approx$ -4%, and reduces the total τ, whereas QED effects increase τ by $\approx$ 12%. It should be emphasized that these are significant contributions and can not be ignored. To compare our result with literature, to the best of our knowledge, we could find only one theoretical calculation for the lifetime, using the model potential calculation [31]. Our FSRCC value, 11.05×10^9 s, is smaller by an order of magnitude. The reason for this discrepancy could be attributed to the fact that Ref. [31] is based on a model potential calculation, whereas the present work uses a fully *ab initio* calculation.

E. Dipole Polarizability

The electric dipole polarizability of an atom or ion is a crucial parameter which governs the interaction with external electric fields, and therefore, can provide insights into various fundamental as well as technological implications [7, 88, 89]. In the context of atomic clocks, α is used in estimating the shift in the clock transition frequency due to black-body radiation (BBR). The BBR shift in clock transition frequency is one of the most dominant frequency shifts for clocks at room temperature, and therefore, contribute heavily to the errors in the clocks. The α for an atom or ion can be computed using the expectation value of the dipole operator as

$$\alpha = -\frac{\langle\widetilde{\Psi}_0|\mathbf{D}|\widetilde{\Psi}_0\rangle}{\langle\widetilde{\Psi}_0|\widetilde{\Psi}_0\rangle}, \tag{20}$$

where $|\widetilde{\Psi}_0\rangle$ is ground state perturbed wavefunction of Sr, obtained using the PRCC theory [37, 43–46].

In Table VI, we present our computed α for the ground state of Sr using PRCC theory. For the analysis of electron correlations, we have provided separate contributions at the different levels of the theory. The contributions from the Breit, QED, and perturbative triples are also listed separately. The term *estimated* represents the cumulative contribution from the orbitals from h, i and j-symmetries. As evident from the table, and as can be expected, the largest contribution to α is from the DF. It contributes about 107% of the recommended value. The DF contribution is computed by replacing PRCC wavefunction $|\widetilde{\Psi}_0\rangle$ in Eq. (20) with a DF wavefunction. The linearized PRCC is observed to increase α by 136% of DF value due to electron correlation effects. The nonlinear terms are observed to have a significant opposite contribution of $\approx$ 18%, reducing the α below LPRCC. As discernible from Fig. 8(a), α is well converged with respect to basis size. The Breit, QED and perturbative triples are observed to have important contributions of -1.2%, 1.3% and 0.5%, respectively, of the total value. Our recommended value, 176.5 a.u, of α is within the experimental error bar of the value 186$\pm$18 a.u. reported in Ref. [90].

In Table VI we compare α from previous theory calculations and experiment. The ground state α for Sr has been calculated using CI [72], CICP [74], CI+MBPT [61, 92], CI+all-order [60], and the coupled-cluster [44, 91, 93, 95, 97, 98] method such as ours. However, as evident from the table, there is a variation in the results using different methods. The average value of α reported in previous calculations other than Ref. [97] is 197 a.u., which is higher than the experimental value [90] by $\approx 5\%$. The α, 186.98, reported in Ref. [97] is closest to the experiment. In terms of methodology, among all the previous calculations, our work is more closer to Ref. [97], however, with a key difference in the implementation of Breit and QED corrections. Our recommended value, 176.5 a.u., is $\approx 5\%$ smaller than Ref. [97]. Our DF value, 156.827 a.u., is however in excellent agreement with the value, 156.83 a.u., reported in Ref. [97]. The Breit and QED corrections from our work are observed to be larger than the corrections -0.09 and -0.01%, respectively, reported in Ref. [97]. In addition, the inclusion of perturbative triples in our work accounts for $\approx 0.5\%$ of the total value. The reason for the difference in α from our previous calculation [44] is attributed to the inclusion of nonlinear terms in PRCC theory in the present work. The difference in the α value from CI+MBPT results [61, 92] could be attributed to the treatment of *core-core* electron correlation to all orders of residual Coulomb interaction in the present work. The CI + all-order calculation [60] accounts for these correlations to all orders, however, using a linearized CC theory, whereas the present work uses a nonlinear CC theory to account for the effects of residual Coulomb interaction. This explains the reason for the difference in α values from present work and CI + all-order calculation [60].

In Table VII we provide the contributions from various correlation terms in PRCC theory. The leading order (LO) contribution is observed from the term $\mathbf{T}_1^{(1)\dagger}D$ + H.c., where it contributes $\approx 115\%$ of the final value. The large contribution is expected, as this term includes the contributions from DF and the dominant core-polarization effects. As discernible from Fig. 8(c), $\approx 48\%$ of the LO contribution comes from the $5s$ valence electrons via the dipolar mixing with $6p$ states.

TABLE VI. The value of α (a.u.) for ground state, $5s^2\ {}^1S_0$, of Sr using PRCC theory. The data available from experiment and other theory calculations are also provided for the comparison.

Method	α
DF	156.826
LPRCC	213.429
PRCC	174.893
PRCC(T)	175.773
PRCC(T)+Breit	173.674
PRCC(T)+Breit+QED	175.597
Estimated	176.471
Recommended	176.50 ± 2.65
Other cal.	197.8[a], 198.85[b], 202[c], 197.14(20)[d], 193(13)[e], 190[f], 197.2[g], 201.2[h], 198.9[i], 193.2[j], 190.82[k], 202.02[l], 186.98(85)[m]
Expt.	186(15)[n]

[a]Ref.[74]-CICP,
[b]Ref.[91]- RCCSD,
[c]Ref.[92]-CI+MBPT,
[d]Ref.[60]- CI+all-order,
[e]Ref.[65]- B-spline configuration interaction with a semi-empirical core-polarization model potential,
[f]Ref.[93]-CCSD,
[g]Ref.[61]-CI+MBPT,
[h]Ref.[94]- Semi-empirical approach using model potential,
[i]Ref.[95]-DK-CCSD(T),
[j]Ref.[96]-Model potential with a hard core and the correct large-r coulombic behavior,
[k]Ref.[44]-PRCC,
[l]Ref.[72]-DFCP+RCI,
[m]Ref.[97]-CCSD
[n]Ref.[90]-Expt.,

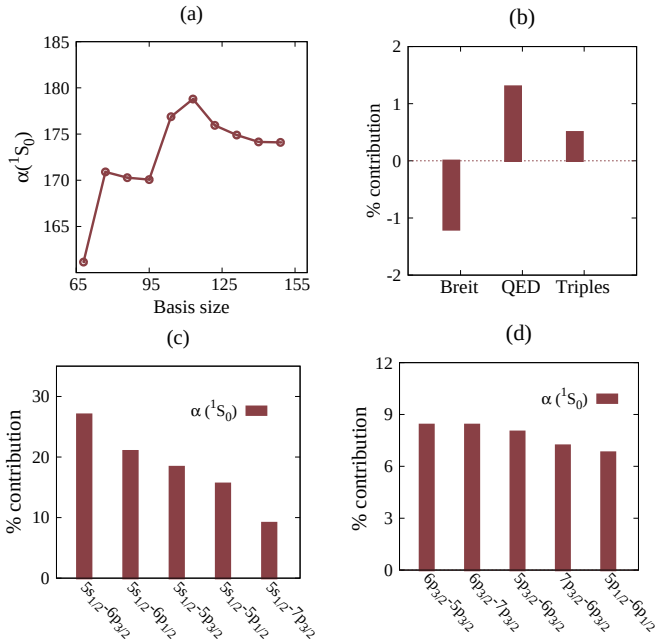

FIG. 8. (a) The convergence of α as a function of basis size, (b) contributions from the various corrections to the polarizability, (c) five largest percentage contributions from core orbitals to LO term $\mathrm{T}_1^{(1)\dagger}\mathrm{D}$, and (d) five leading contributions to NLO term $\mathrm{T}_2^{(1)\dagger}\mathrm{DT}_2^{(0)}$ (in a.u.) from virtual-virtual orbital pairs.

TABLE VII. Termwise contributions to α (a.u.) from different terms in PRCC theory.

Terms + h. c.	α
$\mathbf{T}_1^{(1)\dagger}\mathbf{D}$	201.4959
$\mathbf{T}_1{}^{(1)\dagger}\mathbf{D}T_2^{(0)}$	−11.9852
$\mathbf{T}_1{}^{(1)\dagger}\mathbf{D}T_1^{(0)}$	−17.2535
$\mathbf{T}_2{}^{(1)\dagger}\mathbf{D}T_1^{(0)}$	10.0744
$\mathbf{T}_2{}^{(1)\dagger}\mathbf{D}T_2^{(0)}$	18.5295
Normalization	1.1485
Total	174.8931

In the remaining, $\approx 34\%$ and 9% of contributions arise from the dipolar mixing with $5p$ and $7p$ states, respectively. The next-to-leading order (NLO) term, $\mathrm{T}_2^{(1)\dagger}\mathrm{DT}_2^{(0)}$, contributes $\approx 11\%$ of the total value, highlighting the importance of pair-correlation effects in closed-shell systems. As discernible from Fig. 8(d), we observed dominant contributions from $5p-6p$ and $6p-7p$ virtual-virtual pairs.

F. Isotope shift

In Table VIII, we present our FSRCC results on normal mass shift (K^{NMS}), specific mass shift (K^{SMS}), and field shift (F_{s}) factors for the clock transition ($5s^2\ {}^1S_0 \rightarrow 5s5p\ {}^3P_0$) and two intercombination lines ($5s^2\ {}^1S_0 \rightarrow 5s5p\ {}^3P_1$ and $5s^2\ {}^1S_0 \rightarrow 5s5p\ {}^3P_1$) of Sr. In addition, awe also compute and provide the results from MCDF calculations for analysis and comparison of electron correlation effects. Since MCDF and FSRCC treat electron correlation in fundamentally different ways, their comparison provides valuable insights into the interplay of many-body effects in Sr. The FSRCC theory, being an all-order relativistic many-body approach, serves as a rigorous benchmark for assessing the accuracy and reliability of the MCDF results.

The MCDF results were obtained using RIS4 [107] module interfaced with GRASP2K[56]. We accounted for *core-valence* and *valence-valence* correlations by allowing single and double replacements of the electrons. While *valence-valence* correlation describe the coupling among outer shell electrons, *core-valence* correlation captures the interplay between inner and outer shells. To achieve a balanced description of correlation effects, a multireference framework was adopted, where we used dominant configurations $\{5s^2,\ 5p^2,\ 5s4d\}$ (even-parity) and $\{5s5p,\ 4d5p\}$ (odd-parity) in the configuration space. The active orbital space was extended up to $\{12s12p7d\}$ for even- and $\{12s12p6d\}$ for odd-parity configurations. The FSRCC results were, however, obtained using an in-house code [54]. For this, we used a converged basis set with 131 orbitals ($19s$, $17p$, $17d$, $14f$, and $8g$) in active space and a model space restricted to $5s^2$ and $5s5p$ configurations to ensure the computational tractability while retaining essential correlation effects.

For NMS, to the best of our knowledge, there are no experimental results for ${}^1S_0$ - ${}^3P_0$ and ${}^1S_0$ - ${}^3P_1$ transitions. However, for ${}^1S_0$ - ${}^1P_1$ transition, we could find two experimental results [104, 106]. As evident from the table, the NMS factor obtained from our MCDF calculations show a good agreement with the semi-empirical value for all the transitions. However, our FSRCC results are different than both MCDF and semi-empirical values. The reason for this is attributed to the more accurate treatment of electrons correlations in FSRCC theory.

For the FS factor, as can be observed from the table, there is a large variation in the reported experimental data, and moreover, they have large errors. We find, the differences of $\approx 16\%$ and 151% in the smallest and largest reported experimental values for ${}^1S_0$ - ${}^3P_1$ and ${}^1S_0$ - ${}^1P_1$ transitions, respectively. Our MCDF results for ${}^1S_0$ - ${}^3P_1$ and ${}^1S_0$ - ${}^1P_1$ transitions differ from that of Ref. [102] by $\approx 15\%$ and 18%, respectively. The reason for this could be attributed to the differences in the configuration space considered and correlation treatment. Our FSRCC result for ${}^1S_0$ - ${}^3P_1$ transition lies within the experimental uncertainty of reported value in Ref. [103]. For ${}^1S_0$ - ${}^1P_1$ transition, like the case of ${}^1S_0$ - ${}^3P_1$, it is consistent with [103], however, in general on the higher side of other experimental values.

The calculation of SMS factor is the most challenging among all the three isotope shifts factors. The reason for this is the two-body nature of the SMS operator, which complicates the angular momentum coupling for two-valence systems. As evident from the table, the reported SMS factors from previous calculations and experiments exhibit large variations in both sign and magnitude. Also, the reported experi-

TABLE VIII. The normal mass shift (GHz-amu), specific mass shift (GHz-amu) and field shift (MHz fm^{-2}) factors of Sr calculated using MCDF and FSRCC theories. We have also provided the data from other theory calculations and experiments for comparison.

State/Transition	$K^{\rm NMS}$			$K^{\rm SMS}$			$F_{\rm s}$		
	MCDF	FSRCC	Oth. results	MCDF	FSRCC	Oth. results	MCDF	FSRCC	Oth. results
$^1S_0$ - $^3P_0$	-237.02	-405.72	-235.33^a	-323.61	-576.67		-812.01	-1260.43	
$^1S_0$ - $^3P_1$	-239.94	-352.06	-238.63^a	-322.92	-20.03	191.1^b, 189.96 ± 12.87^c, -469.22^d, -0.151^e, 190.90 ± 119.32^f	-814.34	-1240.95	-1034 ± 24^b, -953.18 ± 67.42^c, -1055.36^d, -955.06^e, -1106 ± 165^f
$^1S_0$ - $^1P_1$	-357.79	-332.62	-357.12^a, -357.21^g, 356.9^i	-104.37	47.39	-41.62 ± 20.81^c, -211.90^e, -42.85 ± 28.57^f, 68.112^g, -67.85 ± 53.57^h, -23 ± 3^i	-764.35	-1234.55	-788.39 ± 102.99^c, -936.33^e, -896 ± 130^f , -806 ± 36^g, 1579 ± 47^h, -628 ± 64^i

[a]Semi-empirically derived result using the relation $K^{\rm NMS}$ = ν/1822.9, where ν is the experimental transition frequency,
[b]Ref.[99]- Expt.,
[c]Ref.[100]- Expt.,
[d]Ref.[101]- First-order perturbative treatment,
[e]Ref.[102]- Multiconfiguration Hartree-Fock (MCHF) theory,
[f]Ref.[103]- Expt.,
[g]Ref.[104]- Expt.,
[h]Ref.[105]- Expt.,
[i]Ref.[106]- Expt.

mental values are from the old measurements and have large errors. For $^1S_0$ - $^3P_1$ transition, our MCDF value -322.92 GHz-amu have the same sign but smaller in magnitude than the calculation [101]. On contrary, among all the reported results, our FSRCC result, -20 GHz-amu, is more closer to the MCDF calculation [102] For $^1S_0$ - $^1P_1$, in terms of magnitude, the FSRCC result is more closer to the experiments than the MCDF values, demonstrating the superior accuracy of the FSRCC approach. Additionally, the sign of our SMS factor is consistent with experiment [104]. The close agreement between the FSRCC results and the best available experimental data highlights the robustness and predictive capability of the FSRCC method for high-precision isotope shift studies.

IV. THEORETICAL UNCERTAINTY

As given in Eqs. (11) and (13), theoretical uncertainty in the computed τ depends on the uncertainties in the E1 and M1 matrix elements, and the energy denominators. Since there are accurate data on the excitation energies from experiments, we have used them in the calculation of lifetime. As experimental results are not available for all the E1 and M1 reduced matrix elements, we have identified four different sources which can contribute to the uncertainties in these matrix elements. The first source of uncertainty is due to the truncation of the basis set in our calculation. As discussed in the basis convergence section, our calculated values of E1 and M1 reduced matrix elements converge well to the order of 10^{-3} or smaller with basis. Since this is a very small change, we can neglect this uncertainty. The second source of uncertainty arises due to the truncation of the dressed Hamiltonian at the second order of $T^{(0)}$ in the properties calculation [46, 62]. In our earlier work [48], using an iterative scheme, we found that the terms with third and higher orders in $T^{(0)}$ contribute less than 0.1%. So, we consider 0.1% as an upper bound from this source of uncertainty. The third source is due to the partial inclusion of triple excitations in the FSRCC theory. Since the perturbative triples account for the leading order terms in triple excitation, the contribution from remaining terms will be small. Based on the analysis from our previous works [37, 45], we estimate the upper bound from this source of uncertainty as 0.72%. The fourth source of uncertainty could be associated with the frequency-dependent Breit interaction which is not included in the present calculation. However, in our previous work [44], using a series of computations using GRASP2K we estimated an upper bound on this uncertainty as 0.13% in Ra. So, for the present work, we take 0.13% as an upper bound from this source. There could be other sources of theoretical uncertainty, such as the higher order coupled perturbation of vacuum polarization and self-energy terms, quadruply excited cluster operators, etc. However, in general, these all have much lower contributions to the properties and their cumulative theoretical uncertainty could be below 0.1%.

The other source of theoretical uncertainty which will contribute to the lifetime of the clock state is the QED corrections at the level of Eqs. (11, 13). To estimate this uncertainty, we refer to the Refs. [108, 109]. In these works, Shabaev and collaborators have computed the one-loop QED corrections to the properties of Cs and Fr. The reported total contribution is about 0.28%. So, based on these works we consider 0.3% as the upper bound from this source of uncertainty. By combining the upper bounds of all the uncertainties, the theoretical uncertainty associated with the lifetime of the clock state is $\approx$ 3.5%. It should, however, be noted that the uncertainty in the value of α is much smaller, about 1.5% [110]

V. CONCLUSIONS

We have employed an all-particle multireference FSRCC theory to investigate the clock transition properties in both Fermionic and Bosonic isotopes of Sr. We have computed the excitation energies, E1 and M1 matrix elements, and the lifetime of the metastable clock states in ^{87}Sr and ^{88}Sr. To account for valence-valence electron correlation more accurately using FSRCC, we used a larger model space consisting of $5s^2$, $5s5p$, $5s4d$, $5s6s$, and $5s6p$ configurations. Moreover, we have implemented the calculation of isotope shifts within the framework of FSRCC theory and have computed isotope shift parameters for clock transition and two intercombination lines in Sr. Furthermore, we employed a PRCC theory to compute the ground state electric dipole polarizability of Sr. To improve the accuracy of the computed properties, we incorporated the corrections from the Breit interaction, self-energy correction, vacuum polarization and perturbative triples to all our calculations. Furthermore, the convergence of the properties were ensured using large bases.

Our calculated excitation energies of low-lying states show a good agreement with experimental results. Our calculated E1, M1 and HFS matrix elements are consistent with previous calculations, however, slightly different because of more accurate treatment of electron correlations in our calculations. Using our calculated E1, M1 and HFS reduced matrix elements, we calculated the lifetime of the metastable clock states for ^{87}Sr and ^{88}Sr. Our calculated lifetime for ^{87}Sr is within the error bar of the experimental results. It should, however, be mentioned that experiments and previous calculations have large errors. For ^{88}Sr, our calculated lifetime is an order of magnitude smaller than the only available calculation [31] using model potential. Our recommended value for ground state α is within the experimental error bar. As can be expected due to more accurate treatment of electron correlations, our FSRCC results on isotope shifts parameters show differences from the MCDF calculations.

From the detailed analysis of electron correlations, we find that the corrections from the Breit interaction, QED effects, and perturbative triples are crucial to get accurate lifetimes of the clock states. The cumulative contributions from Breit interaction and QED effects to the lifetime are observed to be $\approx$ 9% and 1% for ^{88}Sr and ^{87}Sr, respectively. Whereas, perturbative triples are found to contribute $\approx$ 8.3% and 4.5% for ^{88}Sr and ^{87}Sr, respectively. Our calculations also show that, perturbative triples are crucial to get accurate excitation energies.

ACKNOWLEDGMENTS

The authors wish to thank Ravi Kumar and Suraj Pandey for the useful discussion. Palki acknowledges the fellowship support from UGC (BININ04154142), Govt. of India. B. K. M acknowledges the funding support from SERB, DST (CRG/2022/003845). Results presented in the paper are based on the computations using the High Performance Computing clusters Padum at IIT Delhi and PARAM RUDRA facility at IUAC under the National Supercomputing Mission of Government of India.

Appendix A: Convergence table of the properties with basis size

In Table IX, we have shown the convergence trend for E1, HFS and M1 reduced matrix elements for all the transitions considered in the present work. Similarly, Table X shows convergence of dipole polarizability with basis size.

[1] A. D. Ludlow, M. M. Boyd, J. Ye, E. Peik, and P. O. Schmidt, "Optical atomic clocks," Rev. Mod. Phys. **87**, 637–701 (2015).
[2] S. De and A. Sharma, "Indigenisation of the Quantum Clock: An Indispensable Tool for Modern Technologies," Atoms **11**, 71 (2023).
[3] V. A. Dzuba, V. V. Flambaum, and S. Schiller, "Testing physics beyond the standard model through additional clock transitions in neutral ytterbium," Phys. Rev. A **98**, 022501 (2018).
[4] J. C. Berengut, D. Budker, C. Delaunay, V. V. Flambaum, C. Frugiuele, E. Fuchs, C. Grojean, Roni Harnik, R. Ozeri, G. Perez, and Y. Soreq, "Probing new long-range interactions by isotope shift spectroscopy," Phys. Rev. Lett. **120**, 091801 (2018).
[5] M. S. Safronova, "The search for variation of fundamental constants with clocks," Annalen der Physik **531**, 1800364 (2019).
[6] J. D. Prestage, R. L. Tjoelker, and L. Maleki, "Atomic clocks and variations of the fine structure constant," Phys. Rev. Lett. **74**, 3511–3514 (1995).
[7] S. G. Karshenboim and E Peik, *Astrophysics, Clocks and Fundamental Constants, Lecture Notes in Physics* (Springer, New York, 2010).
[8] S. Kolkowitz, I. Pikovski, N. Langellier, M. D. Lukin, R. L. Walsworth, and J. Ye, "Gravitational wave detection with optical lattice atomic clocks," Phys. Rev. D **94**, 124043 (2016).

TABLE IX. Convergence trend of E1, HFS, and M1 reduced matrix elements with basis size.

States	BS-68[a]	BS-77[b]	BS-86[c]	BS-95[d]	BS-104[e]	BS-113[f]	BS-122[g]	BS-131[h]	BS-140[i]	BS-149[j]	BS-158[k]	BS-167[l]	BS-176[l]	BS-185[l]	BS-194[l]	BS-203[l]
E1 reduced matrix elements (in a.u.)																
$\langle {}^1S_0 \|\|\boldsymbol{d}\|\| {}^3P_1\rangle$	0.1495	0.1491	0.1484	0.1473	0.1472	0.1477	0.1482	0.1463	0.1445	0.1440	0.1436	0.1425	0.1409	0.1404	0.1402	0.1398
$\langle {}^1S_0 \|\|\boldsymbol{d}\|\| {}^1P_1\rangle$	5.0088	5.0056	5.0054	5.0064	4.9985	4.9809	4.9544	4.9396	4.9228	4.9109	4.8997	4.8965	4.8969	4.8934	4.8904	4.8894
$\langle {}^1S_0 \|\|\boldsymbol{d}\|\| {}^3P'_1\rangle$	0.3848	0.3859	0.3860	0.3856	0.3829	0.3752	0.3597	0.3510	0.3453	0.3498	0.3471	0.3455	0.3422	0.3384	0.3369	0.3359
$\langle {}^1S_0 \|\|\boldsymbol{d}\|\| {}^1P'_1\rangle$	−2.6055	−2.6116	−2.6137	−2.6150	−2.6072	−2.6035	−2.6117	−2.6136	−2.6136	−2.6139	−2.6170	−2.6189	−2.6195	−2.6213	−2.6219	−2.6222
$\langle {}^3S_1 \|\|\boldsymbol{d}\|\| {}^3P_0\rangle$	2.0494	2.0447	2.0413	2.0388	2.0350	2.0265	2.0157	2.0037	1.9924	1.9835	1.9774	1.9748	1.9703	1.9686	1.9678	1.9673
$\langle {}^3D_1 \|\|\boldsymbol{d}\|\| {}^3P_0\rangle$	−2.5920	−2.5884	−2.5886	−2.5898	−2.5959	−2.5822	−2.5199	−2.4742	−2.4674	−2.4658	−2.4559	−2.4403	−2.4347	−2.4329	−2.4321	−2.4317
HFS Reduced Matrix Elements ($\times 10^{-7}$)																
$\langle {}^3P_1 \|\|t^1\|\| {}^3P_0\rangle$	2.1052	2.1679	2.2239	2.2539	2.2841	2.3210	2.3773	2.4031	2.4215	2.4533	2.4789	2.4904	2.4849	2.4834	2.4789	
$\langle {}^1P_1 \|\|t^1\|\| {}^3P_0\rangle$	1.6078	1.6491	1.6833	1.7064	1.7263	1.7539	1.7941	1.8019	1.8211	1.8643	1.8830	1.8986	1.9099	1.8759	1.8277	
M1 Reduced Matrix Elements (in a.u.)																
$\langle {}^3P_1 \|\|m1\|\| {}^3P_0\rangle$	−1.2035	−1.2027	−1.2022	−1.2019	−1.2054	−1.2074	−1.2083	−1.2090	−1.2112	−1.2122	−1.2129	−1.2125	−1.2123	−1.2127	−1.2131	−1.2132
$\langle {}^1P_1 \|\|m1\|\| {}^3P_0\rangle$	0.2829	0.2833	0.2835	0.2836	0.2806	0.2782	0.2759	0.2742	0.2716	0.2702	0.2692	0.2691	0.2688	0.2684	0.2679	0.2678
$\langle {}^3P'_1 \|\|m1\|\| {}^3P_0\rangle$	0.0830	0.0818	0.0808	0.0800	0.0749	0.0679	0.0597	0.0523	0.0429	0.0370	0.0322	0.0312	0.0290	0.0270	0.0259	0.0253
$\langle {}^1P'_1 \|\|m1\|\| {}^3P_0\rangle$	−0.2609	−0.2616	−0.2619	−0.2622	−0.2598	−0.2582	−0.2576	−0.2568	−0.2548	−0.2532	−0.2525	−0.2526	−0.2526	−0.2524	−0.2521	−0.2519
$\langle {}^1S_0 \|\|m1\|\| {}^3S_1\rangle$	−1.0739	−1.0730	−1.0750	−1.0772	−0.9998	−0.8399	−0.6549	−0.5614	−0.5486	−0.5324	−0.5044	−0.4748	−0.4616	−0.4584	−0.4573	−0.4565
$\langle {}^1S_0 \|\|m1\|\| {}^3D_1\rangle$	−0.0002	−0.0002	−0.0003	−0.0003	−0.0003	−0.0002	−0.0002	−0.0002	−0.0002	−0.0002	−0.0002	−0.0002	−0.0002	−0.0002	−0.0002	−0.0002

[a] Yu. Ralchenko, A. Kramida, J. Reader, and the NIST ASD Team, NIST Atomic Spectra Database (version 4.1), available at http:physics.nist.gov/ asd (National Institute of Standards and Technology, Gaithersburg, MD, 2011)
[b] Basis 68 - 12s, 10p, 10d, 7f, 1g
[c] Basis 77 - 13s, 11p, 11d, 8f, 2g
[d] Basis 86 - 14s, 12p, 12d, 9f, 3g
[e] Basis 95 - 15s, 13p, 13d, 10f, 4g
[f] Basis 104 - 16s, 14p, 14d, 11f, 5g
[g] Basis 113 - 17s, 15p, 15d, 12f, 6g
[h] Basis 122 - 18s, 16p, 16d, 13f, 7g
[i] Basis 131 - 19s, 17p, 17d, 14f, 8g
[j] Basis 140 - 20s, 18p, 18d, 15f, 9g
[k] Basis 149 - 21s, 19p, 19d, 16f, 10g
[l] Basis 158 - 22s, 20p, 20d, 17f, 11g
[m] Basis 167 - 23s, 21p, 21d, 18f, 12g
[n] Basis 176 - 24s, 22p, 22d, 19f, 13g
[o] Basis 185 - 25s, 23p, 23d, 20f, 14g
[p] Basis 194 - 26s, 24p, 24d, 21f, 15g
[q] Basis 203 - 27s, 25p, 25d, 22f, 16g
[r] Basis 212 - 28s, 26p, 26d, 23f, 17g
[s] Basis 221 - 29s, 27p, 27d, 24f, 18g

TABLE X. Convergence trend of α (a.u.) for ground state, $5s^2\ ^1S_0$, of Sr from PRCC calculation as function of basis size.

Basis size	α
Basis-68	161.1397
Basis-77	170.9020
Basis-86	170.2805
Basis-95	170.0681
Basis-104	176.8809
Basis-113	178.7907
Basis-122	175.9380
Basis-131	174.8931
Basis-140	174.1457
Basis-149	174.0953

[9] Ruxandra Bondarescu, Mihai Bondarescu, György Hetényi, Lapo Boschi, Philippe Jetzer, and Jayashree Balakrishna, "Geophysical applicability of atomic clocks: direct continental geoid mapping," Geophysical Journal International **191**, 78–82 (2012).

[10] Tanja E Mehlstäubler, Gesine Grosche, Christian Lisdat, Piet O Schmidt, and Heiner Denker, "Atomic clocks for geodesy," Reports on Progress in Physics **81**, 064401 (2018).

[11] D. S. Weiss and M. Saffman, "Quantum computing with neutral atoms," Physics Today **70**, 44–50 (2017).

[12] D. J. Wineland, J. C. Bergquist, J. J. Bollinger, R. E. Drullinger, and W. M. Itano, "Quantum computers and atomic clocks," in *Frequency Standards and Metrology* (2002) pp. 361–368.

[13] Fritz Riehle, "Towards a redefinition of the second based on optical atomic clocks," Comptes Rendus Physique **16**, 506–515 (2015), the measurement of time / La mesure du temps.

[14] M. S. Grewal, A. P. Andrews, and C. G. Bartone, *Global Navigation Satellite Systems, Inertial Navigation, and Integration* (John Wiley and Sons, New York, 2013).

[15] F.G. Major, *The Quantum Beat: The Physical Principles of Atomic Clocks* (Springer New York, 2013).

[16] Mason C. Marshall, Daniel A. Rodriguez Castillo, Willa J. Arthur-Dworschack, Alexander Aeppli, Kyungtae Kim, Dahyeon Lee, William Warfield, Joost Hinrichs, Nicholas V. Nardelli, Tara M. Fortier, Jun Ye, David R. Leibrandt, and David B. Hume, "High-stability single-ion clock with 5.5×10^{-19} systematic uncertainty," Phys. Rev. Lett. **135**, 033201 (2025).

[17] M. Chwalla, J. Benhelm, K. Kim, G. Kirchmair, T. Monz, M. Riebe, P. Schindler, A. S. Villar, W. Hänsel, C. F. Roos, R. Blatt, M. Abgrall, G. Santarelli, G. D. Rovera, and Ph. Laurent, "Absolute frequency measurement of the $^{40}Ca^+$ $4s\ ^2s_{1/2} - 3d\ ^2d_{5/2}$ clock transition," Phys. Rev. Lett. **102**, 023002 (2009).

[18] T. Lindvall, T. Fordell, K. J. Hanhijärvi, M. Doležal, J. Rahm, S. Weyers, and A. E. Wallin, "$^{88}Sr^+$ optical clock with 7.9 x 10^{-19} systematic uncertainty and measurement of its absolute frequency with 9.8 x 10^{-17} uncertainty," Phys. Rev. Appl. , – (2025).

[19] Nozomi Ohtsubo, Ying Li, Nils Nemitz, Hidekazu Hachisu, Kensuke Matsubara, Tetsuya Ido, and Kazuhiro Hayasaka, "Frequency ratio of an $^{115}In^+$ ion clock and a ^{87}Sr optical lattice clock," Opt. Lett. **45**, 5950–5953 (2020).

[20] S Dörscher, N Huntemann, R Schwarz, R Lange, E Benkler, B Lipphardt, U Sterr, E Peik, and C Lisdat, "Optical frequency ratio of a $^{171}Yb^+$ single-ion clock and a ^{87}Sr lattice clock," Metrologia **58**, 015005 (2021).

[21] Scott A Diddams, Th Udem, JC Bergquist, EA Curtis, RE Drullinger, L Hollberg, Wayne M Itano, WD Lee, CW Oates, KR Vogel, *et al.*, "An optical clock based on a single trapped $^{199}Hg^+$ ion," Science **293**, 825–828 (2001).

[22] Alexander Aeppli, Kyungtae Kim, William Warfield, Marianna S. Safronova, and Jun Ye, "Clock with 8×10^{-19} systematic uncertainty," Phys. Rev. Lett. **133**, 023401 (2024).

[23] Xavier Baillard, Mathilde Fouché, Rodolphe Le Targat, Philip G. Westergaard, Arnaud Lecallier, Yann Le Coq, Giovanni D. Rovera, Sebastien Bize, and Pierre Lemonde, "Accuracy evaluation of an optical lattice clock with bosonic atoms," Opt. Lett. **32**, 1812–1814 (2007).

[24] WF McGrew, X Zhang, RJ Fasano, SA Schäffer, K Beloy, D Nicolodi, RC Brown, N Hinkley, G Milani, M Schioppo, TH Yoon, and AD Ludlow, "Atomic clock performance enabling geodesy below the centimetre level," Nature **564**, 87—90 (2018).

[25] Kazuhiro Yamanaka, Noriaki Ohmae, Ichiro Ushijima, Masao Takamoto, and Hidetoshi Katori, "Frequency ratio of ^{199}Hg and ^{87}Sr optical lattice clocks beyond the si limit," Phys. Rev. Lett. **114**, 230801 (2015).

[26] P. O. Schmidt, T. Rosenband, C. Langer, W. M. Itano, J. C. Bergquist, and D. J. Wineland, "Spectroscopy using quantum logic," Science **309**, 749–752 (2005).

[27] C. W. Chou, D. B. Hume, J. C. J. Koelemeij, D. J. Wineland, and T. Rosenband, "Frequency comparison of two high-accuracy Al^+ optical clocks," Phys. Rev. Lett. **104**, 070802 (2010).

[28] Nicola Poli, MG Tarallo, Marco Schioppo, CW Oates, and GM Tino, "A simplified optical lattice clock," Applied Physics B **97**, 27–33 (2009).

[29] Cédric Delaunay, Roee Ozeri, Gilad Perez, and Yotam Soreq, "Probing atomic higgs-like forces at the precision frontier," Phys. Rev. D **96**, 093001 (2017).

[30] S. Origlia, M. S. Pramod, S. Schiller, Y. Singh, K. Bongs, R. Schwarz, A. Al-Masoudi, S. Dörscher, S. Herbers, S. Häfner, U. Sterr, and Ch. Lisdat, "Towards an optical clock for space: Compact, high-performance optical lattice clock based on bosonic atoms," Phys. Rev. A **98**, 053443 (2018).

[31] Robin Santra, Kevin V. Christ, and Chris H. Greene, "Properties of metastable alkaline-earth-metal atoms calculated using an accurate effective core potential," Phys. Rev. A **69**, 042510 (2004).

[32] Xiaotong Lu, Feng Guo, Yebing Wang, Min Feng, Ting Liang, Benquan Lu, and Hong Chang, "M_F-dependent hyperfine-induced $5s5p\ ^3P_0^o - -5s^2\ ^1S_0$ clock transition rates in an external magnetic field for ^{87}Sr," Phys. Rev. A **108**, 012820 (2023).

[33] Sergey G. Porsev and Andrei Derevianko, "Hyperfine quenching of the metastable $^3P_{0,2}$ states in divalent atoms," Phys. Rev. A **69**, 042506 (2004).

[34] R. Pal, M. S. Safronova, W. R. Johnson, A. Derevianko, and S. G. Porsev, "Relativistic coupled-cluster single-double method applied to alkali-metal atoms," Phys. Rev. A **75**, 042515 (2007).

[35] B. K. Mani, K. V. P. Latha, and D. Angom, "Relativistic coupled-cluster calculations of ^{20}Ne, ^{40}Ar, ^{84}Kr, and ^{129}Xe: Correlation energies and dipole polarizabilities," Phys. Rev. A **80**, 062505 (2009).

[36] H. S. Nataraj, B. K. Sahoo, B. P. Das, and D. Mukherjee, "Reappraisal of the electric dipole moment enhancement factor for thallium," Phys. Rev. Lett. **106**, 200403 (2011).

[37] R. Kumar, S. Chattopadhyay, B. K. Mani, and D. Angom, "Electric dipole polarizability of group-13 ions using perturbed relativistic coupled-cluster theory: Importance of nonlinear terms," Phys. Rev. A **101**, 012503 (2020).

[38] E. Eliav, U. Kaldor, and Y. Ishikawa, "Transition energies of ytterbium, lutetium, and lawrencium by the relativistic coupled-cluster method," Phys. Rev. A **52**, 291–296 (1995).

[39] E. Eliav, U. Kaldor, and Y. Ishikawa, "Transition energies of mercury and ekamercury (element 112) by the relativistic coupled-cluster method," Phys. Rev. A **52**, 2765–2769 (1995).

[40] B. K. Mani and D. Angom, "Fock-space relativistic coupled-cluster calculations of two-valence atoms," Phys. Rev. A **83**, 012501 (2011).

[41] R. Kumar, S. Chattopadhyay, D. Angom, and B. K. Mani, "Fock-space relativistic coupled-cluster calculation of a hyperfine-induced $^1S_0 \rightarrow {}^3P_0^o$ clock transition in Al^+," Phys. Rev. A **103**, 022801 (2021).

[42] Palki Gakkhar, Ravi Kumar, D. Angom, and B. K. Mani, "Fock-space relativistic coupled-cluster calculations of clock-transition properties in Pb^{2+}," Phys. Rev. A **110**, 013119 (2024).

[43] S Chattopadhyay, BK Mani, and D Angom, "Electric dipole polarizability from perturbed relativistic coupled-cluster theory: Application to neon," Physical Review A **86**, 022522 (2012).

[44] S. Chattopadhyay, B. K. Mani, and D. Angom, "Electric dipole polarizability of alkaline-earth-metal atoms from perturbed relativistic coupled-cluster theory with triples," Phys. Rev. A **89**, 022506 (2014).

[45] S. Chattopadhyay, B. K. Mani, and D. Angom, "Triple excitations in perturbed relativistic coupled-cluster theory and electric dipole polarizability of group-IIB elements," Phys. Rev. A **91**, 052504 (2015).

[46] R. Kumar, S. Chattopadhyay, D. Angom, and B. K. Mani, "Relativistic coupled-cluster calculation of the electric dipole polarizability and correlation energy of Cn, Nh^+, and Og: Correlation effects from lighter to superheavy elements," Phys. Rev. A **103**, 062803 (2021).

[47] B.K. Mani, S. Chattopadhyay, and D. Angom, "RCCPAC: A parallel relativistic coupled-cluster program for closed-shell and one-valence atoms and ions in fortran," Computer Physics Communications **213**, 136–154 (2017).

[48] B. K. Mani and D. Angom, "Atomic properties calculated by relativistic coupled-cluster theory without truncation: Hyperfine constants of Mg^+, Ca^+, Sr^+, and Ba^+," Phys. Rev. A **81**, 042514 (2010).

[49] W R Johnson, "Atomic structure theory. lectures on atomic physics," (2007).

[50] I. Lindgren and J. Morrison, *Atomic Many-Body Theory* (Springer, Berlin, 2nd Edition, 1986).

[51] Tomas Brage, Philip G. Judge, Abdellatif Aboussaïd, Michel R. Godefroid, Per Jönsson, Anders Ynnerman, Charlotte Froese Fischer, and David S. Leckrone, "Hyperfine induced transitions as diagnostics of isotopic composition and densities of low-density plasmas," The Astrophysical Journal **500**, 507 (1998).

[52] C. Nazé, E. Gaidamauskas, G. Gaigalas, M. Godefroid, and P. Jönsson, "ris3: A program for relativistic isotope shift calculations," Computer Physics Communications **184**, 2187–2196 (2013).

[53] E Gaidamauskas, C Nazé, P Rynkun, G Gaigalas, P Jönsson, and M Godefroid, "Tensorial form and matrix elements of the relativistic nuclear recoil operator," Journal of Physics B: Atomic, Molecular and Optical Physics **44**, 175003 (2

[54] Palki Gakkhar, D. Angom, and B. K. Mani, "Isotope shifts calculation of one- and two-valence atomic systems using fs-rcc theory," *to be published*.

[55] A. K. Mohanty, F. A. Parpia, and E. Clementi, "Kinetically balanced geometric gaussian basis set calculations for relativistic many-electron atoms," in *Modern Techniques in Computational Chemistry: MOTECC-91*, edited by E. Clementi (ESCOM, 1991).

[56] P. Jönsson, G. Gaigalas, J. Bieroń, C. Froese Fischer, and I. P. Grant, "New version: GRASP2K relativistic atomic structure package," Comp. Phys. Comm. **184**, 2197 – 2203 (2013).

[57] R. E. Stanton and S. Havriliak, "Kinetic balance: A partial solution to the problem of variational safety in dirac calculations," J. Chem. Phys. **81**, 1910–1918 (1984).

[58] O. Zatsarinny and C. F. Fischer, "DBSR_HF: A B-spline Dirac-Hartree-Fock program," Computer Physics Communications **202**, 287 – 303 (2016).

[59] A. Kramida, Yu. Ralchenko, J. Reader, and and NIST ASD Team, NIST Atomic Spectra Database (ver. 5.10), [Online]. Available: `https://physics.nist.gov/asd` [2023, March 8]. National Institute of Standards and Technology, Gaithersburg, MD. (2022).

[60] M. S. Safronova, S. G. Porsev, U. I. Safronova, M. G. Kozlov, and Charles W. Clark, "Blackbody-radiation shift in the Sr optical atomic clock," Phys. Rev. A **87**, 012509 (2013).

[61] S. G. Porsev, Andrew D. Ludlow, Martin M. Boyd, and Jun Ye, "Determination of Sr properties for a high-accuracy optical clock," Phys. Rev. A **78**, 032508 (2008).

[62] B. K. Mani and D. Angom, "Fock-space relativistic coupled-cluster calculations of two-valence atoms," Phys. Rev. A **83**, 012501 (2011).

[63] David Husain and José Schifino, "Kinetic study of Sr ($5\ ^3P_J$) by time-resolved emission $5\ ^3P_1 \rightarrow 5\ ^1S_0$ + hν (λ = 689.3 nm) following dye-laser excitation," J. Chem. Soc., Faraday Trans. 2 **80**, 321–334 (1984).

[64] Ryszard Drozdowski, M Ignaciuk, Jerzy Kwela, and Józef Heldt, "Radiative lifetimes of the lowest $^3P_1$ metastable states of Ca and Sr," Zeitschrift für Physik D Atoms, Molecules and Clusters **41**, 125–131 (1997)

[65] Kai Guo, Guangfu Wang, and Anpei Ye, "Dipole polarizabilities and magic wavelengths for a Sr and Yb atomic optical lattice clock," Journal of Physics B: Atomic, Molecular and Optical Physics **43**, 135004 (2

[66] Alexandre Cooper, Jacob P. Covey, Ivaylo S. Madjarov, Sergey G. Porsev, Marianna S. Safronova, and Manuel Endres, "Alkaline-earth atoms in optical tweezers," Phys. Rev. X **8**, 041055 (2018).

[67] J. F. Kelly, M. Harris, and A. Gallagher, Phys. Rev. A **37**, 2354–2360 (1988).

[68] Masami Yasuda, Tetsuo Kishimoto, Masao Takamoto, and Hidetoshi Katori, "Photoassociation spectroscopy of ^{88}Sr: Reconstruction of the wave function near the last node," Phys. Rev. A **73**, 011403 (2006).

[69] Leszek Glowacki and Jacek Migdalek, "Relativistic configuration-interaction oscillator strength calculations with ab initio model potential wavefunctions," Journal of Physics B: Atomic, Molecular and Optical Physics **36**, 3629 (200

[70] S. G. Porsev, M. G. Kozlov, Yu. G. Rakhlina, and A. Derevianko, "Many-body calculations of electric-dipole amplitudes for transitions between low-lying levels of Mg, Ca, and Sr," Phys. Rev. A **64**, 012508 (2001).

[71] W H Parkinson, E M Reeves, and F S Tomkins, "Neutral calcium, strontium and barium: determination of

f values of the principal series by the hook method," Journal of Physics B: Atomic and Molecular Physics **9**, 157 (1976).
[72] Fang-Fei Wu, Yong-Bo Tang, Ting-Yun Shi, and Li-Yan Tang, "Dynamic multipolar polarizabilities and hyperpolarizabilities of the Sr lattice clock," Phys. Rev. A **100**, 042514 (2019).
[73] S. B. Nagel, P. G. Mickelson, A. D. Saenz, Y. N. Martinez, Y. C. Chen, T. C. Killian, P. Pellegrini, and R. Côté, "Photoassociative spectroscopy at long range in ultracold strontium," Phys. Rev. Lett. **94**, 083004 (2005).
[74] Yongjun Cheng, Jun Jiang, and J. Mitroy, "Tune-out wavelengths for the alkaline-earth-metal atoms," Phys. Rev. A **88**, 022511 (2013).
[75] N Vaeck, M Godefroid, and J E Hansen, "MCHF oscillator strength and lifetime calculations in neutral calcium," Journal of Physics B: Atomic, Molecular and Optical Physics **24**, 361 (1991).
[76] Sergey G. Porsev and Andrei Derevianko, "High-accuracy relativistic many-body calculations of van der Waals coefficients C_6 for alkaline-earth-metal atoms," Phys. Rev. A **65**, 020701 (2002).
[77] J. Mitroy and J.Y. Zhang, "Dispersion and polarization interactions of the strontium atom," Molecular Physics **108**, 1999–2006 (2010).
[78] Yong Liu, Martin Andersson, Tomas Brage, Yaming Zou, and Roger Hutton, "Lifetime calculations for the $5s5p\,^3P_2$ metastable level of ^{88}Sr I," Phys. Rev. A **75**, 014502 (2007).
[79] F. M. Kelly and M. S. Mathur, "Hanle effect in the singlet excited states of the alkaline earths," Canadian Journal of Physics **58**, 1416–1419 (1980).
[80] Jonsson, G and Levinson, C and Persson, Anders and Wahlström, Claes-Göran, "Natural Radiative Lifetimes In the $^1P_1$ and $^1F_3$ Sequences of Sr I," Zeitschrift für Physik A Hadrons and Nuclei, **316**, 255–258 (1984).
[81] D. A. Miller, L. You, J. Cooper, and Alan Gallagher, "Collisional energy transfer between excited-state strontium and noble-gas atoms," Phys. Rev. A **46**, 1303–1309 (1992).
[82] C. Redondo, M. Rayo, Patricia Écija, Durayd Husain, and F. Castano, "Collisional dynamics of low energy states of atomic strontium following the generation of Sr(5s5p $^1P_1$) in the presence of Ne, Kr and Xe," Chemical Physics Letters **392**, 116–122 (2004).
[83] Martin M. Boyd, Tanya Zelevinsky, Andrew D. Ludlow, Sebastian Blatt, Thomas Zanon-Willette, Seth M. Foreman, and Jun Ye, "Nuclear spin effects in optical lattice clocks," Phys. Rev. A **76**, 022510 (2007).
[84] Juan A. Muniz, Dylan J. Young, Julia R. K. Cline, and James K. Thompson, "Cavity-qed measurements of the ^{87}Sr millihertz optical clock transition and determination of its natural linewidth," Phys. Rev. Res. **3**, 023152 (2021).
[85] Sören Dörscher, Roman Schwarz, Ali Al-Masoudi, Stephan Falke, Uwe Sterr, and Christian Lisdat, "Lattice-induced photon scattering in an optical lattice clock," Phys. Rev. A **97**, 063419 (2018).
[86] Jonathan Dolde, Dhruva Ganapathy, Xin Zheng, Shuo Ma, Kyle Beloy, and Shimon Kolkowitz, "Direct measurement of the $^3P_0$ clock state natural lifetime in ^{87}Sr," Phys. Rev. A **112**, 023121 (2025).
[87] Xiao-Tong Lu, Feng Guo, Yan-Yan Liu, Jing-Jing Xia, Guo-Dong Zhao, Ying-Xin Chen, Ye-Bing Wang, Ben-Quan Lu, and Hong Chang, "Determining the lifetime of the $5s5p^3P_0^o$ metastable state in ^{87}Sr from the electric dipole matrix element," Phys. Rev. Appl. **21**, 024042 (2024).
[88] I.B. Khriplovich, *Parity Nonconservation in Atomic Phenomena* (Gordon and Breach Science Publishers, Philadelphia, 1991).
[89] W. C. Griffith, M. D. Swallows, T. H. Loftus, M. V. Romalis, B. R. Heckel, and E. N. Fortson, "Improved limit on the permanent electric dipole moment of ^{199}Hg," Phys. Rev. Lett. **102**, 101601 (2009).
[90] Henry L. Schwartz, Thomas M. Miller, and Benjamin Bederson, "Measurement of the static electric dipole polarizabilities of barium and strontium," Phys. Rev. A **10**, 1924–1926 (1974).
[91] Ivan S. Lim, Markus Pernpointner, Michael Seth, Jon K. Laerdahl, Peter Schwerdtfeger, Pavel Neogrady, and Miroslav Urban, "Relativistic coupled-cluster static dipole polarizabilities of the alkali metals from li to element 119," Phys. Rev. A **60**, 2822–2828 (1999).
[92] SG Porsev and A Derevianko, "High-accuracy calculations of dipole, quadrupole, and octupole electric dynamic polarizabilities and van der waals coefficients C_6, C_8, and C_{10} for alkaline-earth dimers," Journal of Experimental and Theoretical Physics **102**, 195–205 (2006).
[93] Andrzej J. Sadlej, Miroslav Urban, and Odd Gropen, "Relativistic and electron-correlation contributions to the dipole polarizability of the alkaline-earth-metal atoms Ca, Sr, and Ba," Phys. Rev. A **44**, 5547–5557 (1991).
[94] J. Mitroy and M. W. J. Bromley, "Semiempirical calculation of van der waals coefficients for alkali-metal and alkaline-earth-metal atoms," Phys. Rev. A **68**, 052714 (2003).
[95] Ivan S. Lim and Peter Schwerdtfeger, "Four-component and scalar relativistic douglas-kroll calculations for static dipole polarizabilities of the alkaline-earth-metal elements and their ions from Ca^n to Ra^n (n = 0,+1,+2)," Phys. Rev. A **70**, 062501 (2004).
[96] SH Patil, "A simple model potential description of the alkaline earth isoelectronic sequences," The European Physical Journal D-Atomic, Molecular, Optical and Plasma P
[97] Yashpal Singh, B. K. Sahoo, and B. P. Das, "Correlation trends in the ground-state static electric dipole polarizabilities of closed-shell atoms and ions," Phys. Rev. A **88**, 062504 (2013).
[98] B. K. Sahoo and B. P. Das, "Relativistic coupled-cluster studies of dipole polarizabilities in closed-shell atoms," Phys. Rev. A **77**, 062516 (2008).
[99] B.A. Bushaw and B.D. Cannon, "Diode laser based resonance ionization mass spectrometric measurement of strontium-90," Spectrochimica Acta Part B: Atomic Spectroscopy **52**, 1839–1854 (1997).
[100] D Bender, H Brand, and V Pfeufer, "Isotope shifts in transitions between low-lying levels of SrI by laser-atomic-beam spectroscopy," Zeitschrift für Physik A Atoms and Nuclei **318**, 291–298 (1984).
[101] Marita C Chidichimo, "Evaluation of the specific mass shift and field shift in the alkaline-earth Sr atom," Zeitschrift für Physik A Atoms and Nuclei **321**, 549–555 (1985).
[102] A Aspect, J Bauche, M Godefroid, P Grangier, J E Hansen, and N Vaeck, "Experimental and mchf isotope shifts of strongly perturbed levels in CaI and SrI," Journal of Physics B: Atomic, Molecular and Optical Physics **24**, 4077 (199
[103] F. Buchinger, R. Corriveau, E. B. Ramsay, D. Berdichevsky, and D. W. L. Sprung, "Influence of the n=50 shell closure on mean square charge radii of strontium," Phys. Rev. C **32**, 2058–2066 (1985).
[104] C.J. Foot, P.E.G. Baird, M.G. Boshier, D.N. Stacey, and G.K. Woodgate, "Generation of cw 243 nm radiation and application to laser spectroscopy of the strontium isotopes," Optics Communications **50**, 199–204 (1984).
[105] F. Buchinger, E. B. Ramsay, R. E. Silverans, P. Lievens, E. Arnold, W. Neu, R. Neugart, K. Wendt, G. Ulm,

and ISOLDE Collaboration, "Nuclear ground state properties of strontium isotopes by laser spectroscopy," AIP Conference Proceedings **164**, 197–200 (1987).

[106] B.A. Bushaw and W. Nörtershäuser, "Resonance ionization spectroscopy of stable strontium isotopes and ^{90}Sr via $5s^2\ ^1S_0 \rightarrow 5s5p\ ^1P_1 \rightarrow 5s5d\ ^1D_2 \rightarrow 5s11f\ ^1F_3 \rightarrow Sr^+$," Spectrochimica Acta Part B: Atomic Spectroscopy **55**, 1679–1692 (2000).

[107] J. Ekman, P. Jönsson, M. Godefroid, C. Nazé, G. Gaigalas, and J. Bieroń, "RIS 4: A program for relativistic isotope shift calculations," Computer Physics Communications **235**, 433–446 (2019).

[108] V. M. Shabaev, K. Pachucki, I. I. Tupitsyn, and V. A. Yerokhin, "Qed corrections to the parity-nonconserving $6s-7s$ amplitude in ^{133}Cs," Phys. Rev. Lett. **94**, 213002 (2005).

[109] V. M. Shabaev, I. I. Tupitsyn, K. Pachucki, G. Plunien, and V. A. Yerokhin, "Radiative and correlation effects on the parity-nonconserving transition amplitude in heavy alkali-metal atoms," Phys. Rev. A **72**, 062105 (2005).

[110] Ravi Kumar, D. Angom, and B. K. Mani, "Fock-space perturbed relativistic coupled-cluster theory for electric dipole polarizability of one-valence atomic systems: Application to Al and In," Phys. Rev. A **106**, 032801 (2022).